FABRICATION AND CHARACTERIZATION OF CARBON NANOTUBE BASED SUPERCAPACITOR ELECTRODES

A THESIS SUBMITTED TO
THE GRADUATE SCHOOL OF NATURAL AND APPLIED SCIENCES
OF
MIDDLE EAST TECHNICAL UNIVERSITY

BY

ITIR BAKIŞ DOĞRU

IN PARTIAL FULFILLMENT OF THE REQUIREMENTS
FOR
THE DEGREE OF MASTER OF SCIENCE
IN
THE DEPARTMENT OF MICRO AND NANOTECHNOLOGY

APRIL 2016

Approval of the thesis

FABRICATION AND CHARACTERIZATION OF CARBON NANOTUBE BASED SUPERCAPACITOR ELECTRODES

submitted by **ITIR BAKIŞ DOĞRU** in partial fulfillment of the requirements for the degree of **Master of Science in Micro and Nanotechnology Department, Middle East Technical University** by,

Prof. Dr. Gülbin Dural Ünver _____
Dean, Graduate School of **Natural and Applied Sciences**

Prof. Dr. Tayfun Akın _____
Head of Department, **Micro and Nanotechnology**

Assoc. Prof. Dr. Hüsnü Emrah Ünalan
Supervisor, **Metallurgical and Materials Eng. Dept.,METU**_____

Prof. Dr. Raşit Turan
Co-Supervisor, **Physics Dept.,METU** _____

Examining Committee Members:

Prof. Dr. Zeki Aktaş _____
Chemical Engineering Dept., Ankara University

Prof. Dr. Raşit Turan _____
Physics Dept., METU

Assoc. Prof. Dr. Hüsnü Emrah Ünalan _____
Metallurgical and Materials Engineering Dept., METU

Prof. Dr. Caner Durucan _____
Metallurgical and Materials Engineering Dept., METU

Assoc. Prof. Dr. Ali Çırpan _____
Chemistry Dept., METU

Date: *15.04.2016*

I hereby declare that all information in this document has been obtained and presented in accordance with academic rules and ethical conduct. I also declare that, as required by these rules and conduct, I have fully cited and referenced all material and results that are not original to this work.

Name, Last name : Itır Bakış, Doğru

Signature :

ABSTRACT

FABRICATION AND CHARACTERIZATION OF CARBON NANOTUBE BASED SUPERCAPACITOR ELECTRODES

Doğru, Itır Bakış
M.Sc. Department of Micro and Nanotechnology
Supervisor : Assoc. Prof. Dr. Hüsnü Emrah Ünalan
Co-Supervisor: Prof. Dr. Raşit Turan
April 2016, 91 pages

Nanotechnology has started a new era where the nano-sized particles are manipulated. These nano-sized particles have lots of applications in a number of fields. Although carbon is one of the most abundant elements of the Earth or human body, in recent years it get an incredible perspective because of its nano-sized constructions like fullerene, graphene, graphite and carbon nanotubes. Carbon nanotubes are flawless cylinders consists of carbon where their radius are a few nanometers while their lengths are at least in micron range. Along the tube, delocalized electrons can freely move. When there are vertically aligned carbon nanotube forests, they form a desirable structure for energy storage devices as they have high aspect ratio.

In this thesis carbon nanotubes are grown on aluminum foils through chemical vapor deposition method and then performed as supercapacitor electrodes. First, aluminum foils are deposited with catalyst via physical vapor deposition or ultrasonic spray pyrolysis method. Both commercial kitchen foil and pure aluminum foil are used for the carbon nanotube growth and compared. Afterwards, the effects of chemical vapor

deposition parameters are studied. Finally, aluminum foils with CNTs are utilized as supercapacitor electrodes and the flexibility of these electrodes samples are assessed.

Keywords: carbon nanotubes, chemical vapor deposition, supercapacitors, flexibility

ÖZ

KARBON NANOTÜP BAZLI SÜPERKAPASİTÖR ELEKTROTLARIN ÜRETİMİ VE KARAKTERİZASYONU

Doğru, Itır Bakış
Yüksek Lisans, Mikro ve Nanoteknoloji Bölümü
Tez Yöneticisi : Doç. Dr. Hüsnü Emrah Ünalan
Ortak Tez Yöneticisi: Prof. Dr. Raşit Turan
Nisan 2016, 91 sayfa

Nano boyuttaki parçacıklarda değişiklik yaptığımız nanoteknololoji yeni bir çağ başlatmıştır. Nano boyuttaki bu parçacıkların birçok kullanım alanları mevcuttur. Dünya'da ya da insan vücudunda en yaygın elementlerden birisi olan karbon son yıllarda fuleren, grafen, grafit ve karbon nanotüp gibi nano boyuttaki yapılarıyla müthiş bir bakış açısı kazanmıştır. Kusursuz silindirik yapıdaki karbon nanotüpler karbonlardan oluşmaktadır, yarıçapları birkaç nanometre iken boyları mikron mertebesindedir. Yöresizleşmiş elektronlar tüplü yapı boyunca hareket ederler. Dik olarak hizalanmış karbon nanotüp ormanları enerji depolama aletleri için tercih edilen yapılardır çünkü oldukça fazla yüzey alanına sahiplerdir.

Bu tezde kimyasal buhar biriktirme yöntemiyle alüminyum folyo üzerinde büyütülmüş karbon nanotüpler süperkapasitör elektrodu olarak kullanılmıştır. İlk olarak alüminyum folyolar üzerine fiziksel buhar büyütme ya da ultrasonik sprey piroliz yöntemleri ile katalizör kaplanmıştır. Bu amaçla ticari mutfak folyosu ve saf alüminyum folyo kullanılmıştır. Sonrasında kimyasal buhar biriktirme parametreleri

çalışılmıştır. Son olarak alüminyum folyo üzerindeki karbon nanotüpler süperkapasitör elektrodu olarak kullanılmış ve esneklikleri test edilmiştir.

Anahtar kelimeler: karbon nanotüpler, kimyasal buhar biriktirme, süperkapasitörler, esneklik

To Gökay and My Family

ACKNOWLEDGMENTS

First and foremost, I would like to express the deepest appreciation to my advisor, Assoc. Prof. Dr. Hüsnü Emrah Ünalan, for giving me the opportunity to work in his lab. His guidance and great effort helped me to improve myself.

I would like to thank my co-supervisor Prof. Dr. Raşit Turan and my thesis committee members Prof. Dr. Zeki Aktaş, Prof. Dr. Caner Durucan and Assoc. Prof. Dr. Ali Çırpan for the critical reading and evaluation of my thesis. I am also grateful to GÜNAM, where I also had a chance to work in a warm environment.

I would especially like to thank Onur Türel, Batuhan Durukan and Doğa Doğanay for their invaluable support in my studies and being such great friends. I am grateful to Şahin Coşkun for his patience in my studies that brings out my results. I would like to thank the members of NANOLAB, Ece Alpugan, Alptekin Aydınlı, Ayşegül Afal, Ekim Saraç, Sevim Polat, Doğancan Tigan, Orçun Ergün, İpek Bayraktar and Pantea Aurang for always being pleasant to me.

Most importantly, I would like to thank my boyfriend, Gökay Yüksel as every time I see him, he makes me smile. He is the best thing that ever happened to me, not only in METU but also in my whole life. His endless care made the completion of this thesis possible.

Finally I would like to thank my mother Nurcihan, my father Musa, my brother Doğuş and all my family. I have been blessed with this very loving and supportive family.

This work was supported by the Scientific and Technological Research Council of Turkey (TÜBİTAK) under Grant no.113E596.

TABLE OF CONTENTS

LIST OF TABLES

TABLES

LIST OF FIGURES

FIGURES

CHAPTER 1

INTRODUCTION

Energy consumption is indispensable for us as technology progresses. In daily life, there is no moment that electricity is unnecessary to human beings. It became an ordinary scene that people sit in public nearby power plugs to charge their electronics. In addition, there is a rising demand in energy storage devices. These devices enable to save the power till it is necessary to operate a tool. Electronic cars are one of the best and high volume applications of energy storage devices. However, these environmentally friendly electronic cars are limited with their charge capacity and high cost.

Nanotechnology started a new era in multidisciplinary areas. Thanks to developed characterization methods, it became clear that materials in nano-scale have peculiar properties compared to their bulk counterparts. It is quite clear that decreasing the size in such dimensions increases the surface area to volume ratio in a great extent. Hence in nano-range, surface properties start to dominate as the structure now mostly consists of surface atoms. When one considers nanomaterials as a little box, through squeezing the box, electronic properties start to change since it is more difficult to delocalize the electron. On the other hand, quantum states are packed densely and seen as a continuum when the material is in bulk form. Confining the material in spatial directions creates discrete states within these

directions and no electron delocalization is observed. All in all, nanomaterials exhibit size and shape dependent properties.

There are a number of carbon allotropes with distinctly different physical properties due to intriguing hybridization of carbon. For example, when carbon atoms form diamond, this rigid crystal structure does not conduct electricity. However, when the carbon atoms form graphite, electrons can easily move along the graphene planes. Another member of the carbon family, carbon nanotubes (CNTs), are one dimensional (1D) structures with high aspect ratio, high mechanical strength and high thermal and electrical conductivity provided that they are multiwalled in nature.

In today's world, one of the most promising storage devices are supercapacitors; where the nanotechnology is directly applied within the electrodes. Activated carbon with mesopores (pore sizes ranging from 2 to 50 nm) is commercially used in this respect.

In this work, aluminum foils are used as readily available, cheap and conductive substrates and CNTs are grown on foils through chemical vapor deposition (CVD) method. CNT covered aluminum foils are then utilized as supercapacitor electrodes. For the CNT growth, aluminum foils are first deposited with catalyst via both physical vapor deposition and ultrasonic spray pyrolysis methods. Both commercial kitchen foil and pure aluminum foil are used for the CNT growth. Within the CVD method, effects of catalyst type and thickness, temperature, annealing process, pressure and gas concentrations are examined. Scanning (SEM) and transmission electron microscopy (TEM), Raman spectroscopy and Brunauer-Emmet-Teller surface area analysis methods are utilized for the characterization of the synthesized CNTs and for the comparison of the experimental results. Afterwards, aluminum foils with CNTs are utilized as supercapacitor electrodes and electrochemical measurements are conducted. Finally, the flexibility of these electrode samples is tested.

CHAPTER 2

CARBON NANOTUBES

2.1 Nanotechnology

Nanotechnology involves working at the atomic and molecular levels within the length scale of 1 – 100 nm, in order to understand materials properties or create new materials, devices as well as systems with fundamentally distinct properties and functions due to their small structure [1]. As size decreases, quantum confinement effects are observed, where nanoparticles have different properties than their bulk counterparts. Moreover, the surface area to volume ratio increases abruptly.

2.2 Carbon Materials

Molecular binding configurations affect the structure of the material and its properties. Carbon provides a wide variety of crystal structures due to its different bonding configurations originated from hybridization [2]. Carbon has an atomic number of 6, and an electron configuration of [He]$2s^2 2p^2$. The difference between 2s and 2p state is very small and easy to overcome with an external perturbation. As a result, four valence electrons can easily mix and form new hybrid orbitals [3].

The mixture of a single 2*s* orbital with *n* number of 2*p* orbitals, where *n* =1, 2 and 3 is called sp^n hybridization. Each carbon atom has (*n*+1) σ bonds. These hybridization structures are shown in Figure 2.1.

The sp^3-hybridization forms a tetrahedral geometry, where the angle between the orbitals is 109.5° as shown in Figure 2.1 (a). Since all the valence electrons bond strongly to the neighboring carbon atoms, they form a diamond structure [4]. Due to this tight bonding, diamonds are electrical insulators. Diamond is considered to be one of the hardest known material because of its rigid lattice structure, as shown in Figure 2.2 (a).

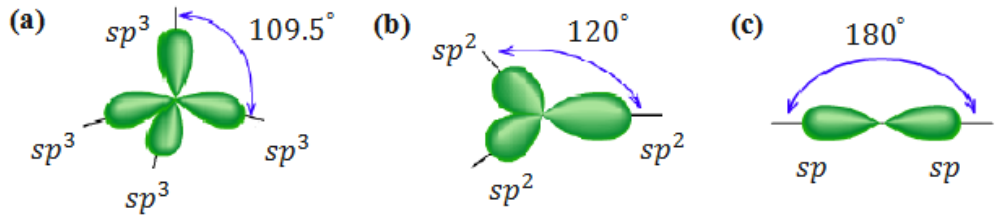

Figure 2.1 (a) sp^3, (b) $sp^2 and$ (c) sp hybridized carbon atoms.

The combination of one *s* orbital and two *p* orbitals with an angle of 120°generates the sp^2-hybridization (Figure 2.1 (b)), where the third *p* orbital forms a π-bond. When a number of sp^2 hybridized carbon atoms combine with each other, they contribute to a planar assembly. Due to resonance, unhybridized *p* orbitals form rings of delocalized electrons that freely move along this planar surface. These delocalized electrons make these structures very good electrical conductors [5]. A typical sp^2 hybridized structure is graphite. It consists of parallel layers as shown in Figure 2.2 (b). Each layer is held together by van der Waals forces, which makes graphite a soft material. It is a three

dimensional allotrope of carbon. The monolayer of the graphite is called graphene. In graphene, each carbon atom is bonded to three other carbon neighbors. This one atom thick structure has unusual properties as being the thinnest and strongest known material. This two-dimensional allotrope consists of arranged hexagons like a honeycomb as shown in Figure 2.2 (c). Electrons in graphene can be described as massless Dirac fermions; thus, have a high electronic mobility [6]. CNTs can be considered as a graphene sheet rolled into a tube along a given direction as shown in Figure 2.2 (d). Because of the quantum confinement effects, electron wave function is quantized along the peripheral direction and electrons can move along only in one direction, which is along the length of CNTs, forming a 1D material [7]. Another allotrope of carbon is fullerene. It is rolled-up graphene sheet to a full circle with sp^3 patches, as shown in Figure 2.2 (e). From the physical point of view, because of discrete energy states they can be thought as zero dimensional [8].

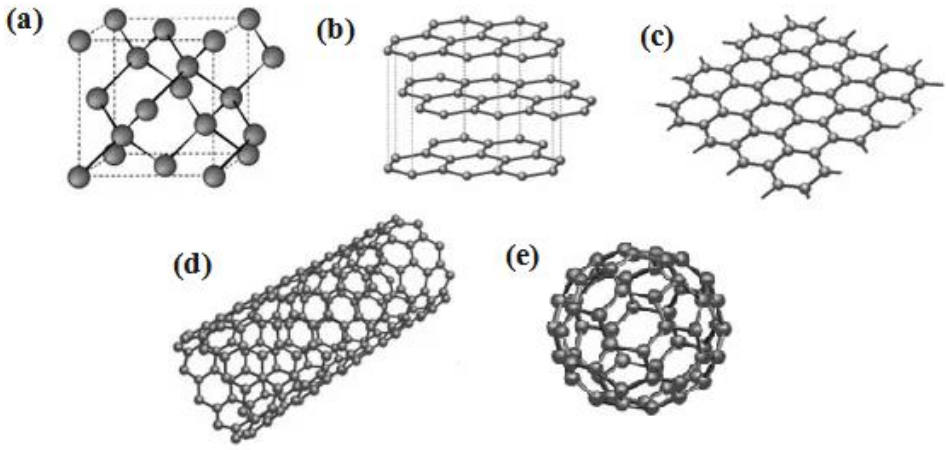

Figure 2.2 Schematics of different carbon allotropes: (a) diamond, (b) graphite, (c) graphene, (d) carbon nanotube and (e) fullerene [5].

2.3 Carbon Nanotubes (CNTs)

CNTs are discovered by Sumio Iijima in 1991, while he was working on graphitic carbon sheets [9]. Not long after the discovery of CNTs, it is understood that they have extraordinary properties like being quite strong, hard, electrically and thermally conductive [10]. Moreover, they have a high aspect ratio; their diameters are as small as a few nanometers; while they can be as long as hundreds of microns [11]. These properties make them potentially useful in a number of applications. One of the fascinating properties of CNTs is their structure. They have honeycomb lattice, which form a helical structure with nanometer sized diameters. This helicity along with nanometer sized diameter changes the electronic density of states, so CNTs get a unique electronic character [12]. The unit cell of a hexagonal structure has two carbon atoms; hence, there are even numbers of delocalized electrons [13]. In a hexagonal structure, each carbon atom bonds to three nearest neighbor atoms and a graphene sheet have a symmetric structure. Rolling up this sheet differs the distances between nearest neighbor atoms from each other [14]. As a result, single walled CNTs may be metallic or semiconducting according to their rolling directions; named chirality in terms of tube diameter d and chiral angle θ as shown in Figure 2.3 (a). A chiral vector C_h can be defined as the distance between two lines along the tube axis, where they separate from graphene. When these two crystallographically equivalent sites are connected, they form a cylinder. This vector can also be constructed by lattice translation indices (n, m) and basic vectors (a_1,a_2).

$$C_h = na_1 + ma_2 \tag{2.1}$$

The zigzag direction can be defined as when m is equal to 0 as shown in Figure 2.3 (b). The chiral angle, θ, can be defined as the angle between chiral vector and zigzag

direction. As a result, we get zigzag CNTs when m=0 and θ=0°, as shown in Figure 2.4 (a). When n=m and θ=30°, armchair nanotubes are observed as shown in Figure 2.4 (b). All other types, when 0<θ<30° as shown in Figure 2.4 (c), are chiral tubes. Armchair single walled CNTs are metallic. On the other hand, zigzag and chiral single walled CNTs are semimetals when

$$n\text{-}m = 3i \quad (i \text{ is an integer and } n \neq m) \tag{2.2}$$

Otherwise they are semiconductors.

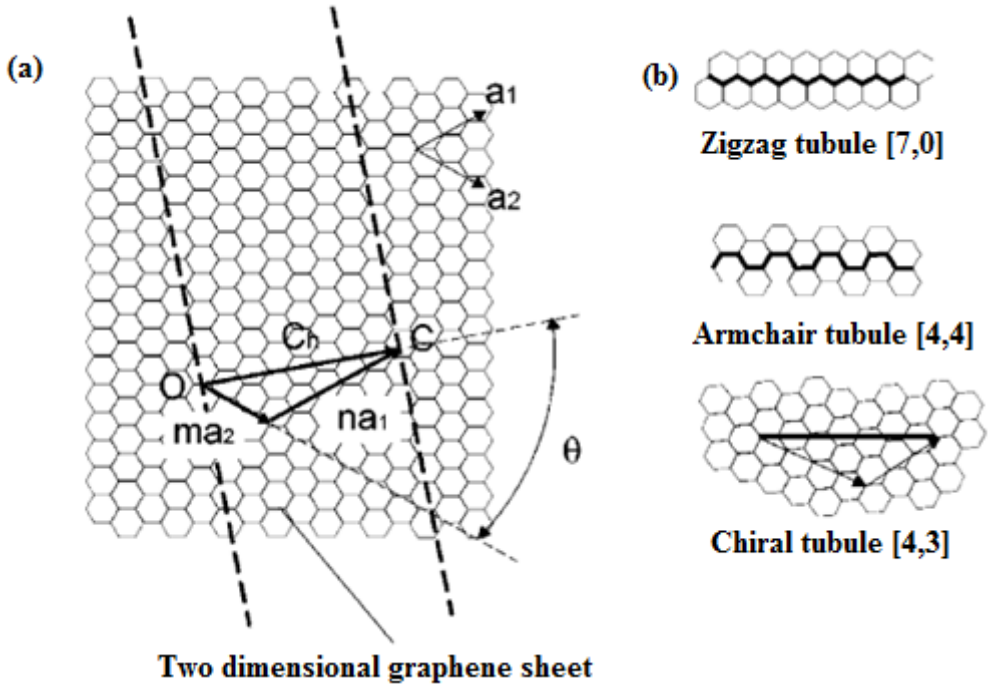

Figure 2.3 Schematics showing (a) chiral vector C_h on a graphene sheet and (b) direction of zigzag, armchair and chiral tubules [15].

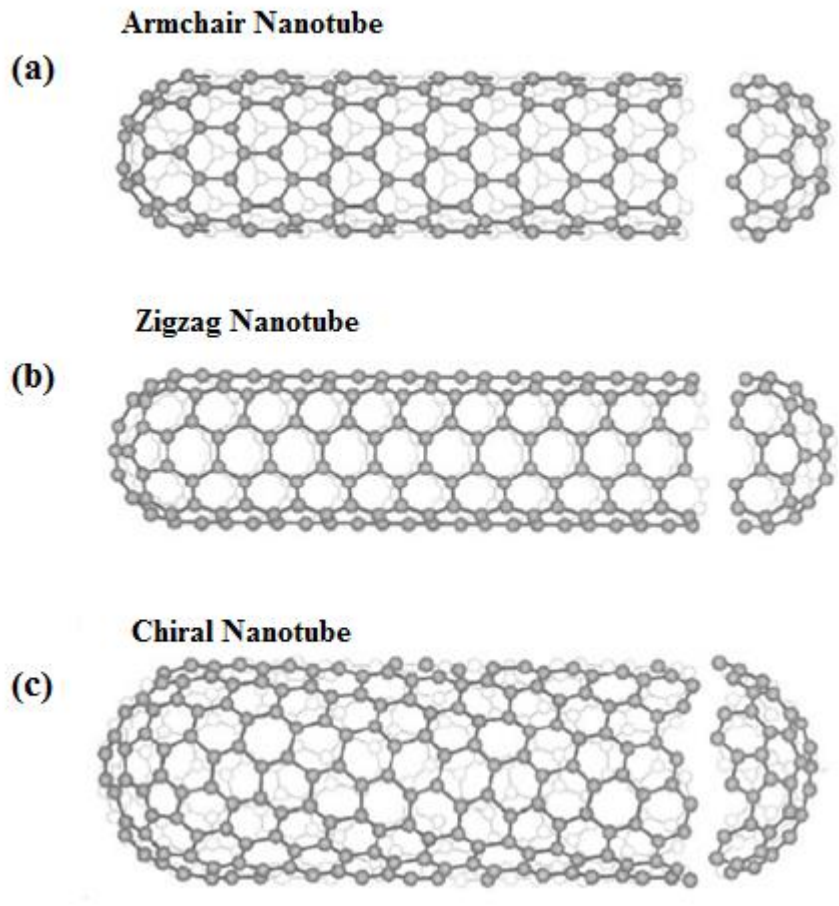

Figure 2.4 Schematics showing (a) armchair, (b) zigzag and (c) chiral CNTs [15].

In addition to their chirality, CNTs can be classified according to their number of walls. Although there are many other types, normally CNTs can be categorized as single walled (SWNT) and multiwalled nanotubes (MWNTs). SWNTs consist of only one graphene sheet as shown in Figure 2.5 (a). Their electronic properties vary according to their chirality. On the other hand, MWNTs consist of multiple layers of rolled graphene sheets, which are arranged in concentric tubes as shown in Figure 2.5 (b). The spacing between these two layers is about 0.34 nm. Each nanotube cylinder has

different helicities and their inter-layer coupling is negligible [13]. MWNTs behave metallic. Their diameters range up to a hundred nanometers.

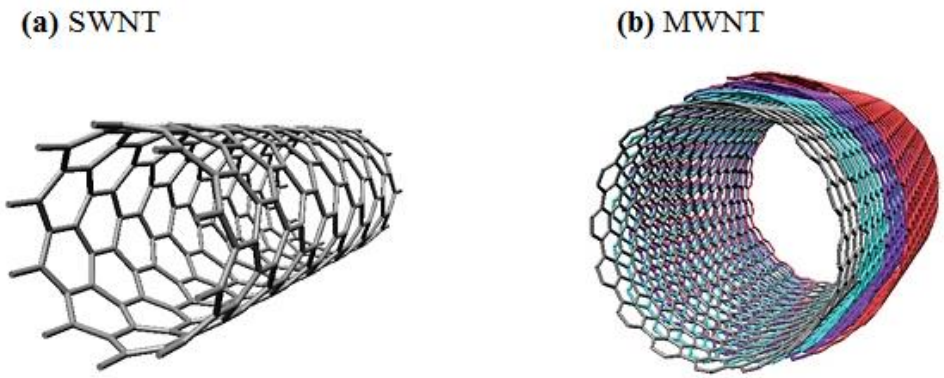

Figure 2.5 Schematics of (a) SWNT and (b) MWNT [16].

2.4 Synthesis Methods of CNTs

CNT synthesis can be considered as the self-assembly of carbon atoms using metal catalysts. There are three common techniques to synthesize CNTs. These are arc-discharge, laser ablation and chemical vapor deposition (CVD) methods [17].

2.4.1 Arc Discharge

This method is based on the arc-vaporization of two graphite electrodes placed horizontally as shown in Figure 2.6. The distance between these two rods is about a few millimeters and the anode may contain metal catalyst particles [18]. The process occurs in a low pressure environment filled with an inert gas. When a voltage of about 20V is applied across the electrodes, a high temperature discharge is observed and

evaporated carbon atoms are deposited on the other electrode in the form of CNTs [19]. Although this process is quite simple, it needs high purification.

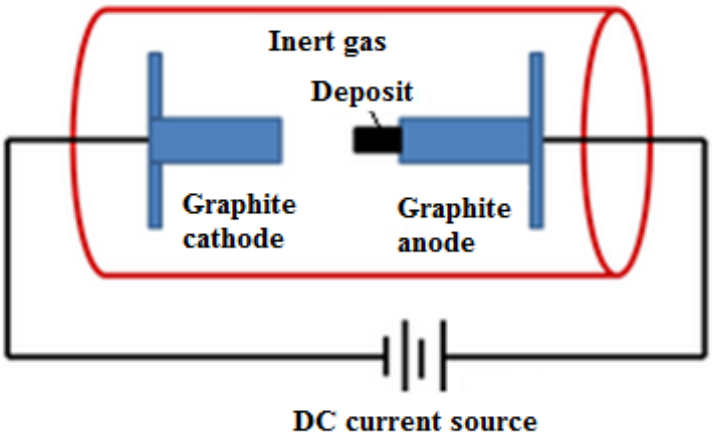

Figure 2.6 Schematic representation of the arc discharge set-up.

2.4.2 Laser Ablation

Laser ablation process utilizes a laser beam to vaporize the carbon atoms of a graphite target. This process is similar to arc discharge method since it is necessary to vaporize a graphite source. This target graphite is placed at around 1200°C tube furnace under an inert gas atmosphere [20]. This system also includes a cooled collector, which collect the condensed carbon atoms and grown CNTs as shown in Figure 2.7. The inert gas flows carry the CNTs through the chamber to the cooled collector.

Both arc discharge and laser ablation necessitate a lot of energy, since temperature should be high to evaporate carbon atoms from the target. Because of this reason, CNTs grown via these methods are highly crystalline and contain less sidewall defects. Although the CNTs produced with laser ablation method have higher purity than those produced in the arc discharge process, they also necessitate purification [19].

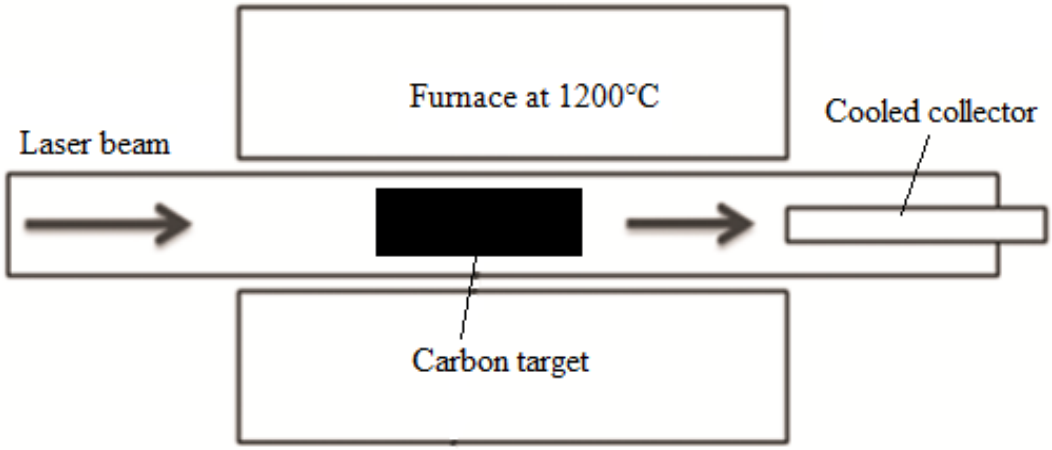

Figure 2.7 Schematic representation of the laser ablation set-up.

2.4.3 Chemical Vapor Deposition (CVD)

In CVD process, gases are introduced into a deposition chamber, where they react and form the desired structure at a solid surface. This method is quite useful for CNT synthesis directly on a substrate and less energy hungry when compared to arc discharge and laser ablation methods. This is because, synthesis temperature is only 600-1000°C [21]. CNTs in this method are produced from the decomposition of hydrocarbon vapor over a metal catalyst [10].

In CVD method, first the metal catalyst deposited substrates are placed into a vacuum chamber as shown in Figure 2.8. Metal catalyst can be in the form of a thin film or nanoparticle. Thin films, during the heating stage, divide into islands because of the thermal expansion mismatch between the thin film and the substrate. During heating, an inert gas is used to prevent oxidation of the nanosized metal catalyst. In a typical cold-wall system, a showerhead directly faces the substrates. It is used to mix the gases

properly and release it onto the substrates [10]. Moreover, all gases sent into the chamber are heated with a graphite stage placed over the substrate holder and homogeneous gas distribution is provided through the holes on this layer. Carbon source gases (typically hydrocarbons) are introduced into the chamber once the growth temperatures are reached. Catalyst metal nanoparticles react with this precursor and form metal carbide. Because of the melting point of nanoparticles are far lower than their bulk phase, CNT formation can be achieved at low temperatures. As a result, metal carbides are observed in quasi-liquid phase in this stage. As the carbon source gas is continuously introduced, metal carbides become unstable. This is because; excessive number of carbon atoms is solved within the metal carbide. By means of concentration and temperature gradients, supersaturated carbon atoms begin to precipitate around metal nanoparticles [22]. These precipitated carbon atoms form a tubular structure as demonstrated in Figure 2.9. Finally, the volatile by-products leave the system by the flow of other gases. System can then be lowered to room temperature under constant flow of an inert gas and then can be opened to collect the samples.

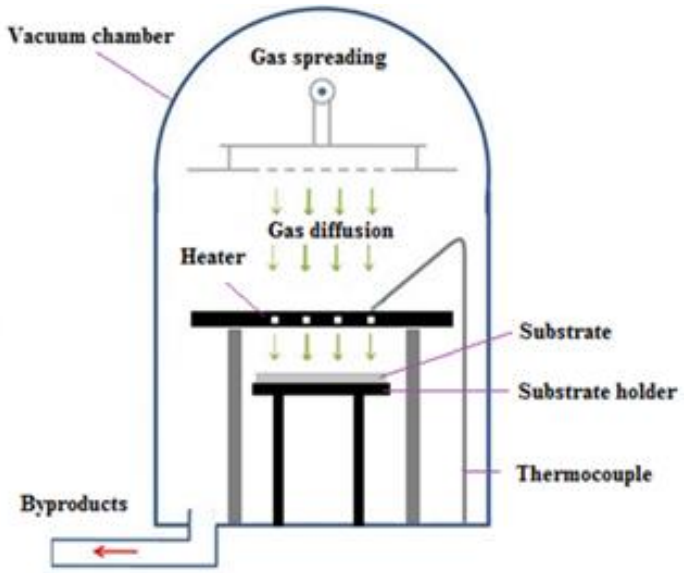

Figure 2.8 Schematic representation of the CVD set-up used in the experiments.

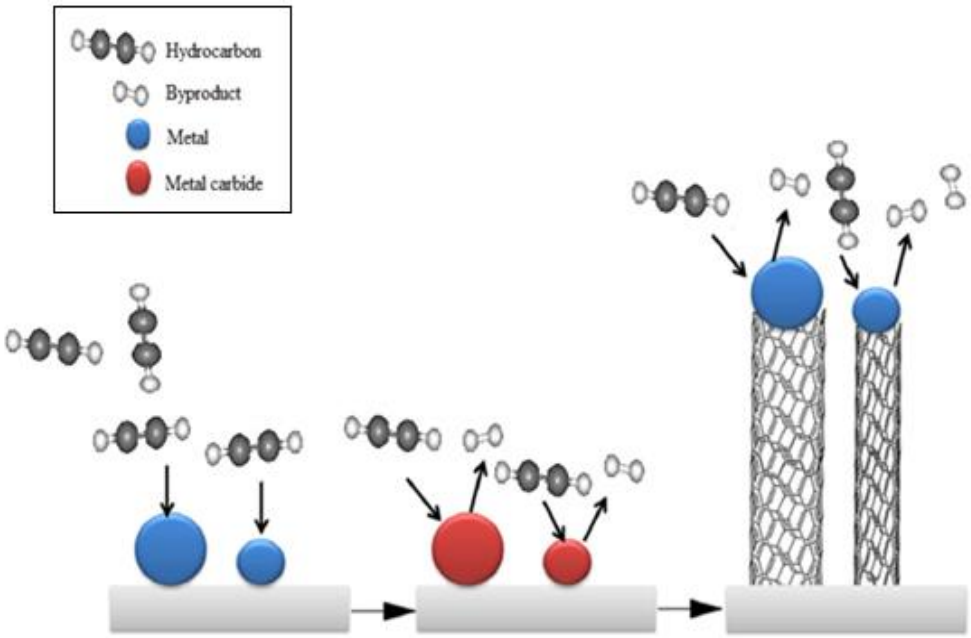

Figure 2.9 Schematics of CNT formation by the CVD method [22].

2.5 Controlling the morphology of CNTs by CVD

CVD growth of CNTs is very suitable for many applications since one can grow CNTs directly on a number of substrates. Synthesis of CNTs over large areas is also possible, which makes CVD method unique and economic. This method also enables the synthesis of patterned CNTs on predefined regions [23].

CNT growth by CVD method proceeds by two steps, namely catalyst preparation and CNT growth. The former affects the reconstruction of the catalyst thin film into islands, while the latter generates CNTs around these islands. Both steps dictate the morphology of the CNTs.

2.5.1 Catalyst Analysis

CNT growth is the result of self-organization of carbon atoms around the metal nanoparticles. Hence, metal nanoparticles can be considered as a template, where gaseous carbon atoms are decomposed and CNT nucleation occurs. The surface of these catalytic particles has a direct influence on the CNT growth [24]. The catalyst is usually deposited as a thin film on the substrate with a predetermined thickness. When this catalyst is exposed to high temperatures as an initial step of CVD, annealing occurs and the metal atoms gather and form metal nanoparticles. Ideally one CNT grows on each nanoparticle [24]. The size of these nanoparticles determines the final diameter of the CNTs. When the CNT formation starts, metal nanoparticles saturate the dangling bonds of CNTs at the edge and stabilize them [25]. As the thickness of the initial thin film increases, the final diameters of the CNTs also increase. It is also possible to grow a few CNTs on a large nanoparticle. On the other hand, thinner initial thin films result in the formation of less and smaller nanoparticles leading to sparse CNT growth as shown in Figure 2.10 [26].

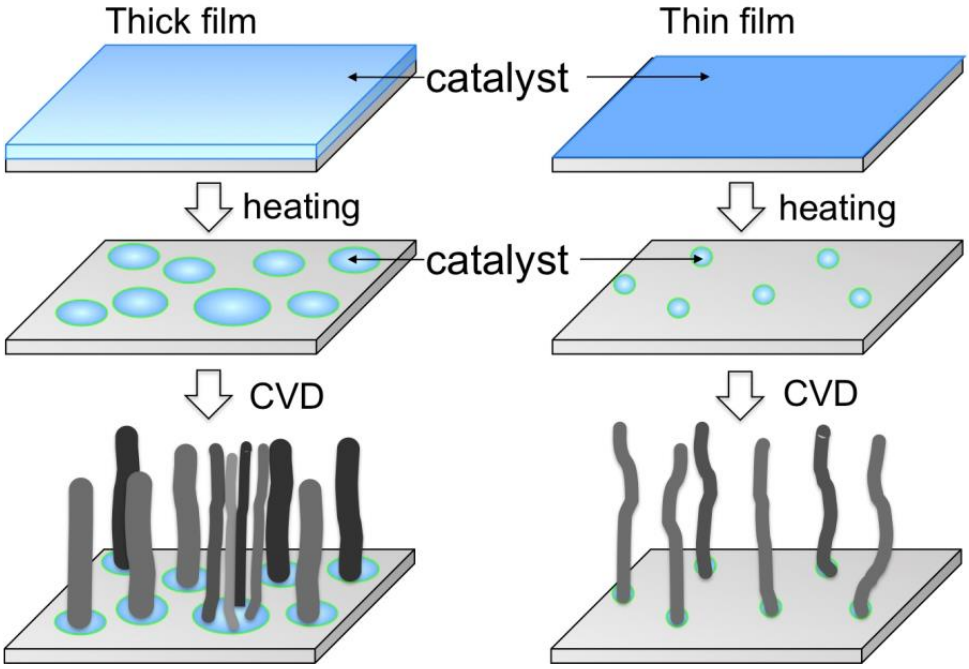

Figure 2.10 The effect of catalyst thickness on CNT density [26].

Two different growth models can be observed following the introduction of CNT precursor. When the catalyst and substrate interaction is weak, hydrocarbon decomposes on top of the metal, carbon precipitates towards the bottom of the metal, pushing the metal up, named as tip growth, as shown in Figure 2.11 (a). On the other hand, when the catalyst and substrate interaction is strong, carbon precipitation cannot push the metal up. Instead, carbon atoms diffuse to the topside of the metal, where the nucleation of CNTs is observed, named as base growth that can be seen in Figure 2.11 (b) [27]. The growth stops when the metal nanoparticle is fully covered with excess carbon, known as catalyst poisoning [10].

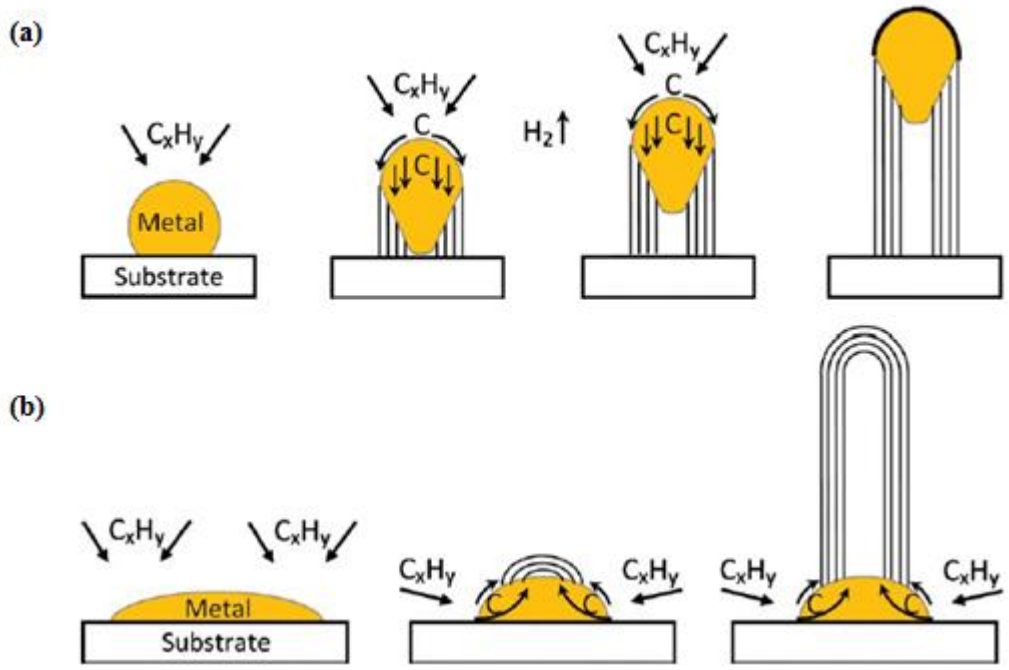

Figure 2.11 Schematics of growth mechanisms of CNTs: (a) tip-growth model and (b) base-growth model [10].

As the mass ratio of CNTs to catalyst increases, aligned CNT growth can be observed resulting from the high packing density. It is valuable to grow vertically aligned carbon nanotube (VACNT) forests instead of a few lateral CNTs on a substrate for many applications [28]. To obtain densest forests, the diameter of the metal nanoparticles should be reduced; hence, thickness of the catalyst should be decreased. While the catalyst particle size becomes smaller, carbon adsorption by the catalyst participate gets enhanced and CNT growth rate increases [29]. On the other hand, as the thickness of the catalyst decreases further, it is likely that the catalyst particles diffuse into the support layer [30]. As a result, it is necessary to find the optimum thickness for catalyst layer as well as the support layer. In addition to catalyst thickness, CVD parameters should also be optimized to grow the VACNT forests. Upon the aligned CNT growth, it is possible to modify their surface and generate a variety of device structures [31].

For CNT growth on a substrate, transition metal catalysts (preferentially nickel, iron and cobalt) are used. To coat the substrate with metal catalyst, solutions that include transition metals can be prepared or physical deposition techniques can be used as direct coating methods [23]. The latter is easier and more controllable since it is difficult to adjust the thickness of the metal thin film by solution-based methods. The thickness of the substrate has no significant influence on catalyst and carbon interaction. When the substrate has high surface energy, catalyst diffusion towards the substrate can be observed. To prevent this, diffusion barrier layers with low surface energies can be deposited as a support layer between the substrate and catalyst [24]. Two catalyst deposition methods, namely physical vapor deposition and ultrasonic spray pyrolysis method are discussed below.

2.5.1.1 Physical Vapor Deposition (PVD)

In PVD process, the material used to be coated vaporizes and then condenses in the form of a thin film on the desired substrate material in a vacuum environment. In the evaporator, small chunks of coating material are placed into a tungsten boat, where the temperature of the boat is increased through current flow, finally evaporating the coating material. The substrate is placed upside-down to enable the condensation on the substrate surface, as shown in Figure 2.12. The reason why the evaporation takes place in a vacuum environment is to prevent contamination, oxidation and to transmit the evaporated atoms easily from the source to the substrate. For this reason, depositions are generally conducted at a vacuum level of 10^{-6}-10^{-7}Torr. Following the achievement of the desired vacuum level, applied current to the boat is increased to melt and then vaporize the substance.

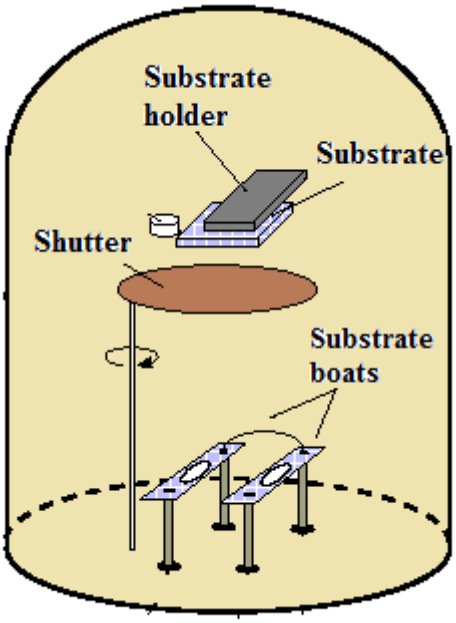

Figure 2.12 Schematic of the PVD system [32].

Within the PVD system, there exists a shutter positioned just below the substrate holder. It is used to control the thickness of the deposited material. In addition, it is also used to prevent freshly evaporated relatively low purity metal. The substrate holder rotates to allow the deposition of a uniform thin film. Thickness of the deposited thin film is controlled through a thickness monitor attached to the PVD system.

2.5.1.2 Ultrasonic Spray Pyrolysis (USP) Method

An ultrasonic atomic nozzle is used to atomize and spray the desired solution in USP method. The nozzle is usually kept a few centimeters away from the substrate, which is heated for the volatilization of the carrying solvent. An automated x-y stage is used to deposit homogeneous thin films over large areas. A schematic of the USP system is

shown in Figure 2.13. Unlike PVD, USP method can be performed in air, so it is a cheap and fast method.

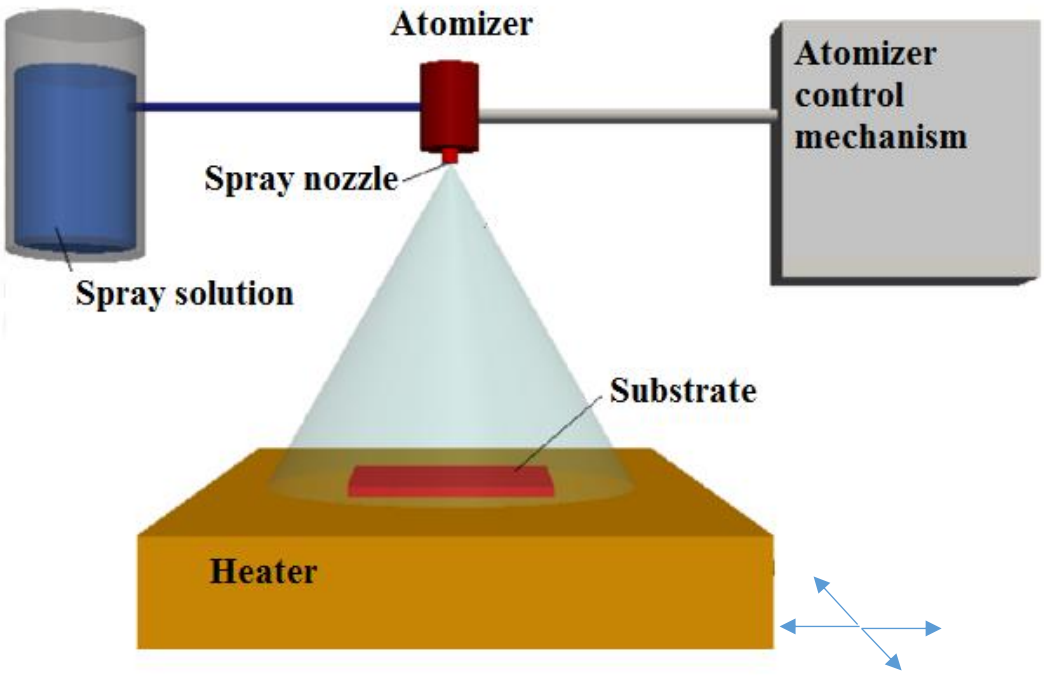

Figure 2.13 Ultrasonic spray pyrolysis equipment used for the deposition of the catalyst [33].

In this system, the precursor has to condense at the same time it reaches the surface of the substrate. If the solvent evaporates and precursor turns into a solid phase before it reaches the substrate, undesired particles can be formed on the substrate instead of thin film structure. As opposed to this situation, if evaporation of the solvent occurs later, drop marks can be observed on the substrate surface. To prevent such problems, it is

essential to adjust the solution volume, substrate surface, spraying rate, heater temperature and the distance between the heater and the nozzle. Optimization of the heater temperature prevents the diffusion of catalyst towards the substrate or formation of drop marks. Moreover, if the spraying rate is not fast enough, solution accumulates inside, coagulating the nozzle, which leads to non-uniform results.

2.5.2 CVD parameters

To get high density VACNTs, it is necessary to equate the source gas flow rate to the CNT formation rate. Hence, it is essential to control the growth rate and avoid the factors that slow down or stop the growth process, such as surface reactions on the catalyst and catalyst poisoning by amorphous carbon [34]. Prior to growth as discussed, a thin film support and catalyst layer is deposited onto the substrates, followed by the placement of substrates into the CVD chamber.

2.5.2.1 The Effect of Growth Pressure

Upon loading the substrates, CVD chamber is generally pumped down to pressures below 10^{-2} mbars using a mechanical pump [35]. This is necessary to prevent catalyst oxidation during processing. Following achievement of a base pressure, inert gases are introduced (typically argon or nitrogen) with a known flow rate and this determines the growth pressure [10]. When the pressure decreases, the mean free path of gases increase. This situation decreases the possibility of collisions to the target inside the chamber [36]. As the pressure gets lower, carbon precursor rate decreases and they diffuse slower to the catalyst. Such a situation prevents catalyst poisoning [37]. On the other hand, at high pressures the carbon precursors gather on the catalyst particles with higher concentration. As the termination rate of carbon atoms overcome the CNT

formation rate, the catalyst particles lose their activity in a short time resulting in a reduced CNT yield [38].

2.5.2.2 The Effect of Annealing

The annealing of the catalyst, as a pretreatment, can be achieved through increasing the chamber temperature and introducing some etching gases like hydrogen. Higher the concentration of hydrogen, catalyst nanoparticle formation rate from the thin metal layer increases [22]. Moreover at high temperatures, beside the etching rate, catalyst particles start to migrate, which increases the diameters and decrease the density of resulting catalyst particles [39]. These situations result in a decrease in CNT density without crowding [40]. Hydrogen also plays a reducing role on the catalyst particles [41].

2.5.2.3 The Effect of Growth Temperature

A source gas is introduced usually when the optimum growth temperature is reached. Higher growth temperatures result in the formation of CNTs with lower defect densities. Temperature is a limiting factor in the type of substrate material. Moreover, the temperature directly affects the gas flow rate and reaction rate. When the temperature is not high enough, the catalytic decomposition of carbon precursors may be quite slow to form the CNTs or decelerates the CNT growth rate. [42, 43]. On the other hand, when the temperature is too high, catalyst surface diffusion or even evaporation can be observed, both of which suppresses the CNT growth [44].

2.5.2.4 The Effect of Gas Flow Rate

In addition to temperature, carbon source gas flow rate affects the formation of CNTs. For the nucleation of CNTs on the catalyst nanoparticles formed during annealing stage, there is an optimum source gas flow rate. When the gas flow rate is too low, deactivation of these catalyst nanoparticles can be observed. On the contrary, when the source gas flow rate is too high, nanoparticles can be poisoned [43]. In such situations, hydrogen is used to dilute the carbon source gas and prevent catalyst poisoning [45]. Hydrogen gas etches the CNTs and forms hydrocarbons, in case of too high flow rates. In this case, the CNT growth stops [46]. These clearly indicate that there is an optimum ratio of hydrogen to precursor gas flow rate during the CNT growth stage.

2.5.2.5 Growth Process

The growth of CNT lasts till the *i)* poisoning of the catalyst particles by carbon or *ii)* CNT etching by hydrogen or *iii)* cutting the source gas flow. If the density of the catalyst nanoparticles can be set properly through optimization, VACNTs growth can be achieved as the result of steric hindrance between the rising CNTs [47]. It is also important that the byproducts leave the system especially during and after the CNT growth process. Hydrogen gas has a big influence on that, since it prevents the deposition of amorphous carbon.

2.6 CNT Synthesis on Aluminum Foils by CVD

In terms of low density and high conductivity; aluminum is the third most abundant element in the world. In addition to these properties, aluminum is an ideal substrate for CNT growth. CNTs grown on metallic foils, aluminum foil in particular, are widely used in electrochemical devices. CNTs on aluminum foils show good cyclic stability

and low resistance that make them perfect electrodes for energy storage devices [48]. Although the melting point of aluminum is not as high as most of the other substrate types, direct growth of CNTs on aluminum foils can be achieved through controlled CVD parameters. On the other hand, aluminum foils are very flexible imparting flexibility to the devices they are utilized. Heating aluminum increases its reactivity and may cause catalyst diffusion towards the substrate. To prevent this, a support layer can be deposited between the catalyst and the substrate [49]. On the other hand, aluminum also have a natural oxide layer on its surfaces, where catalyst deposition without a support layer can be directed with less effort [21].

2.7 CNT Applications

CNTs perfect bond structure makes them quite strong both chemically and mechanically. On the other hand, CNTs free π-bonds and small diameter provide excellent electronic features. Electron transport along the length of the tube without scattering allows them to carry extraordinary current densities [50]. Together with the capability of direct growth on various substrates over defined regions and high aspect ratios, CNTs are appealing for many applications. Some of them are discussed below.

2.7.1 Field Emission Devices

Field emission properties of CNTs enable the realization of cold cathodes for a variety of vacuum devices. For instance, miniaturized X-Ray sources for both medical and industrial applications can be fabricated utilizing CNT cold cathodes. Field emission can be considered as the extraction of electrons from a sharp solid under vacuum, where they accelerate towards the anode under the effect of electric field. Usually phosphor arrays are placed at the anode and upon electrons strike the phosphor, visible light is produced [51]. Smaller the radius of the emitting tips, higher the enhancement

of the electric field. Since CNTs have small radii, high local fields can be created, easily ejecting large number of electrons [50]. High electrical and thermal conductivity of CNTs also play a role in this application.

2.7.2 Field Effect Transistors (FETs)

SWNTs can be used as a channel between source and drain contacts in field effect transistors. Since it is possible to control the length and diameter of the SWNTs and since they can carry high current densities, miniaturized devices can be developed using SWNTs, which are faster than the conventional silicon based devices [52]. It is also possible to make a device where the metal-semiconductor junction formed from only carbon atoms since SWNTs can be both metallic and semiconducting in nature. This prevents diffusion along the junction since both the metallic and the semiconducting side constitutes of only carbon [53].

2.7.3 Biomedical applications

CNTs can be used for drug delivery, where the drug is placed inside or attached to the surface of the tube. In addition, they can arrive to the target organ without affecting the rest of the body and in particular the healthy cells [54].

2.7.4 Electrochemical devices

CNTs have a high aspect ratio and high surface to volume ratio; therefore, they have a high potential to store charges. Furthermore, they are conductive and mechanically robust as required by an ideal electrode material [50]. An electrochemical device will be further discussed in this thesis.

CHAPTER 3

SUPERCAPACITORS

Capacitors are energy storage devices that operate through accumulation of charges on their parallel plates and creating an electrostatic field between them. Since the charge storage by capacitors is a physical process, it is highly reversible [55]. Basically, a conventional capacitor is made up of two conductors separated by an insulator called dielectric as shown in Figure 3.1.

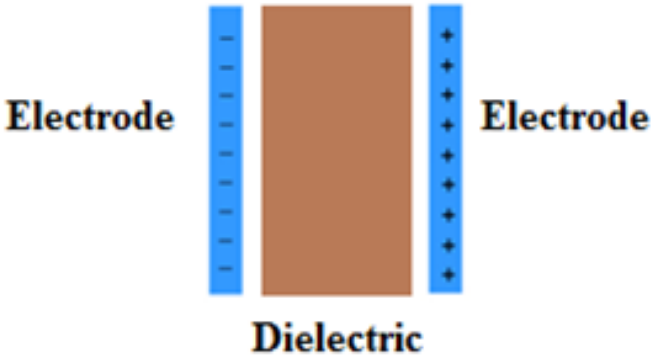

Figure 3.1 Construction of a conventional capacitor

The capacitance is proportional to the area of the conductor plates and inversely proportional to distance of the separation of the plates. So the capacitance is;

$$C = \frac{\mathcal{E}\, A}{d} \tag{3.1}$$

,where C is the capacitance, $\mathcal{E}$ is the dielectric constant, A is the area of the electrodes and d is the distance between the electrodes. Large plates can store more charge and low dielectric thickness values give smaller potential difference.

Working principles of the supercapacitors have some similarities to those of conventional capacitors. However, supercapacitors incorporate electrodes with much higher surface areas and much thinner dielectrics that decrease the distance between the electrodes to have higher energy density. The prefix of "super" comes from the higher order of magnitude of energy storage than conventional capacitors [56]. The construction of supercapacitors consists of an electrode, electrolyte and a current collector [57]. Overall performance of supercapacitors is determined by the physical properties of both the electrode and the electrolyte materials [58]. There is also a membrane, which separates, positive and negative electrodes (as shown in Figure 3.2) and it is called as the separator. These separators prevent shorts between the electrodes at the same time allowing diffusion of ions within the electrolyte solution [57].

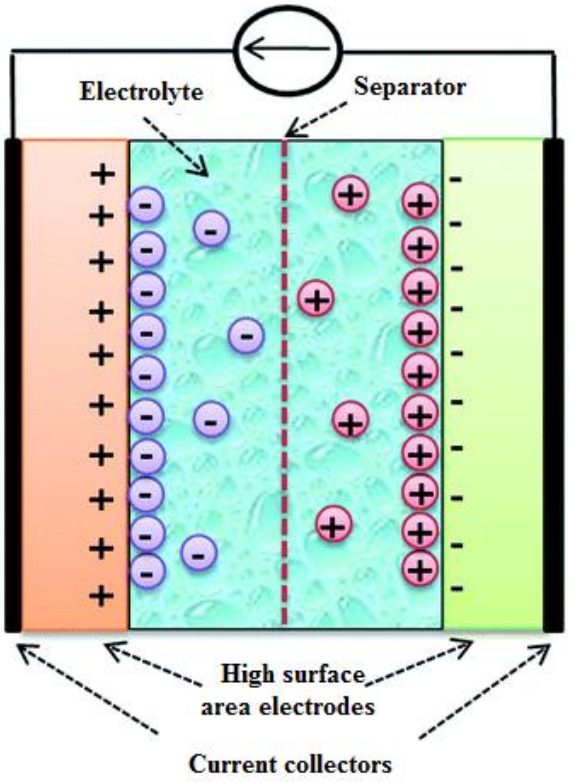

Figure 3.2 Construction of a supercapacitor [59].

Supercapacitors are also named as electric double layer capacitors (EDLC) because when an electric potential is applied to the electrodes, a potential difference is created at the electrode and electrolyte interface. Once the electrode is positively charged, negative ions inside the electrolyte are positioned at the electrode surface, and vice versa. This situation generates an electrode-electrolyte interface. This interface represents a capacitor, while a complete cell can be considered as two capacitors in series. Moreover, this double layer interface distance is reduced quite a lot, which also increases the capacitance. This distance within the atomic range speeds up the transfer of ions between the electrode and the electrolyte [56]. Likewise, as the size of the pores

on the electrodes increases, the penetrated electrolyte volume inside these pores also increases [60].

There are two types of supercapacitors that are electrical double layer capacitors and pseudocapacitors. These two types are explained below.

3.1 Electrical double layer capacitors

Electrical double layer capacitors (EDLCs) take the advantage of the electrostatic interaction between the electrode and the electrolyte. When an electric potential is applied to the polarizable and high surface area electrodes, oppositely charged ions inside the electrolyte are attracted and sited at their surface [61]. At the interface between the electrode and the electrolyte, a double layer is established. There is no charge transfer through this interface; accordingly, the storage process is non-Faradaic [62]. Hence, the ion transfer to or from the electrode surface generates the charge-discharge mechanism that is highly reversible and rapid.

Along with the surface area and conductivity, pore morphology, electrolyte properties and ion size also affect the total capacitance. Even though enlarging the pore volume relative to ion size increases the ion diffusivity toward the electrode, neighboring charges may decrease the specific capacitance by their overlapping electric field [63]. In other words, pore size of the electrode also alters the charge-discharge mechanism [60]. As mentioned in Chapter 2, carbonaceous materials are highly conductive and stable. Besides, they offer controllable structure, all of which are unique properties to be used as supercapacitor electrodes [56]. There are numerous carbonaceous materials that can be used as supercapacitor electrodes, such as activated carbons, CNTs, carbon fibers, graphene and carbon aerogels. All of which have different effects on the overall capacitance [58].

The nanoscale tubular morphology of CNTs offers low electrical resistivity [64]. Along with their porous structure, CNTs might advance the charge diffusion through their central channels. Entangled CNTs offer slower ion and electron movement due to their complex structure that prevents the ion diffusion to each CNT. Conversely, VACNT based electrodes offer higher performance since they have more available surface area, as shown in Figure 3.3. As the VACNTs get denser, much higher capacitance is observed [58].

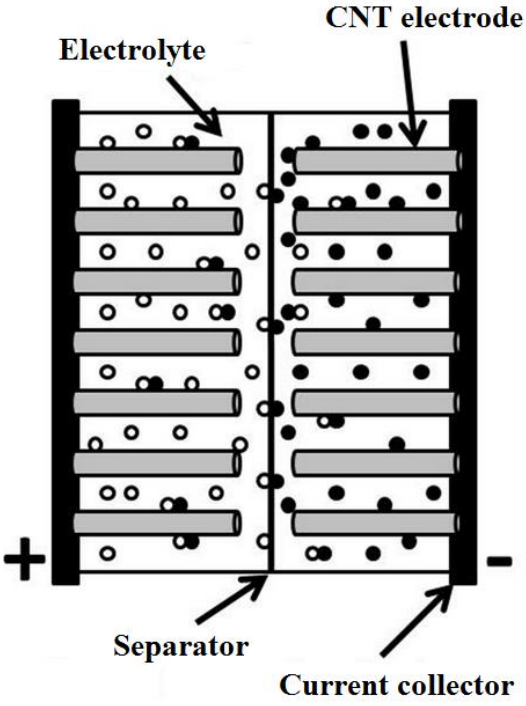

Figure 3.3 VACNT based supercapacitor construction [65].

3.2 Pseudocapacitors

Pseudocapacitors accumulate the charge by way of reversible Faradaic redox reactions. There is an electron transfer reaction at the electrode-electrolyte interface. In other words, redox reaction behaves as a charge-discharge mechanism. Pseudocapacitance is mostly determined by the chemical affinity of electrode materials to absorb ions [66]. Unlike EDLCs, in pseudocapacitors, electrodes not only interact with the electrolyte at their surface but also nearby them [67]. So far, transition metal oxides and conducting polymers are the most widely used electrode materials that display pseudocapacitive behavior [68]. Redox reactions may disrupt the electrode enlarging or contracting them, which is unfavorable for electrode health and operation [67]. To prevent such problems, composite materials can be produced with mechanically strong materials like those used in EDLC electrodes.

CHAPTER 4

EXPERIMENTAL PROCEDURE

The aim of this study is to grow CNTs on conducting surfaces to operate them as supercapacitor electrodes. To be able to get high capacitance, CNTs should be as dense as possible. Thus, VACNTs are preferred. In this study, aluminum foils are utilized as substrates for the direct synthesis of CNTs. The growth method used is CVD. Prior to CNT growth, aluminum foils were deposited with iron catalyst by means of both physical vapor deposition (PVD) and ultrasonic spray pyrolysis (USP) methods.

4.1 CNT Synthesis on Foils

Aluminum foils are soft, flexible, ductile and cheap. They also possess good conductivity. Two types of aluminum foils were used in this work. They were pure (Alfa Aesar, 0.025 mm thick, 99.45% metal basis) and commercial kitchen foils (Koroplast, about 0.018 mm thick). Foils were first cleaned with acetone (99.8%), isopropanol (99.8%) and distilled water (18.3 MΩ) sequentially, through simple immersion to these solvents for 10 minutes each. Soon after, foils were dried in a furnace at 80°C. Following this cleaning, aluminum foils were deposited with catalyst to be able to grow CNTs through CVD.

4.1.1 Catalyst Deposition Methods

Two different catalyst deposition routes, such as PVD and USP were investigated.

4.1.1.1 Physical Vapor Deposition (PVD)

In this method, aluminum was first deposited onto the foils with a thickness of 10-20 nm. For the deposition of the catalyst onto aluminum foils, Nanovak NVTH-350 thermal evaporator was used. Right after, this sample was kept in air environment for a day to oxidize the deposited aluminum, which would act as a barrier layer preventing catalyst diffusion into the substrate. Following the oxidation process, iron catalyst (2.6 nm thick iron film) was deposited through a second PVD step. At the end, foils were annealed at 500°C for 1 hour for the oxidation of the catalyst.

4.1.1.2 Ultrasonic Spray Pyrolysis (USP) Method

To deposit iron catalyst onto aluminum foils, a $5x10^{-3}$ M solution containing iron chloride ($FeCl_3.6H_2O$, 97%) and ethanol was prepared and deposited via USP method. Aluminum foils (8 cm × 6 cm) were placed on the heater set to 155°C and deposited with catalyst. Ultrasonicated solution was sprayed from a distance of 5.25 cm. Heater was mounted on an x-y stage to allow homogeneous deposition of the catalyst onto foils. Since aluminum has a native oxide layer, it was not necessary to deposit a support layer in case of USP. It was noticed that this native oxide layer prevents the diffusion of the catalyst towards the substrate, making this method quite practical. Following the USP deposition of the catalyst, foils were annealed in a furnace at 500°C for 1 hour. This process was repeated for both the pure and kitchen foils.

4.1.2 CNT Synthesis on Foils by CVD Method

Following the catalyst deposition either by USP or PVD, foils were loaded to the CVD system. An Aixtron - Nanoinstruments Black Magic II plasma enhanced CVD system (as seen in Figure 4.1 (a)) was used for the CNT synthesis. The system was fully computer controlled, which allowed precise control over the growth parameters improving the reproducibility of the growth results. Within the system, it is possible and very simple to alter the growth parameters like temperature, gas flow rates and pressure at any moment. For the CNT growth, first the substrates were placed on the stage that is located beneath a porous graphite layer, as shown in Figure 4.1 (b). Next, the system was enclosed by a belljar, as shown in Figure 4.1 (c) to generate a vacuum environment. The substrates were exposed to an etching gas, hydrogen (H_2) and the graphite layer was rapidly heated with a rate of 200°C/min. A thermocouple in direct contact with the graphite layer is used to monitor the temperature. Gases were sent through a showerhead, which homogeneously mixes and sends them over the samples. H_2 gas was used during the whole growth cycle. Well-arranged holes on the heated graphite layer allowed uniform gas distribution over the substrate as well.

Once the desired temperature is reached and the samples were kept there and annealed for the desired amount of time, acetylene (98.5% purity, C_2H_2) gas was sent to the system. At the end of annealing step, catalyst particles were formed on the substrate surface. C_2H_2 gas thermally dissociated through its transit towards the substrate surface and the dissociated gas molecules reacted with the fresh catalyst particles initiating the CNT growth. Subsequently, temperature was slowly increased to a maximum point (~630°C) where the foils stayed intact. Once the maximum temperature was reached, all parameters were kept constant for a desired period of time, called as the growth time. At the end, the flow of C_2H_2 and H_2 gases were stopped

and the system was cooled to room temperature under nitrogen (N_2) gas. Finally, the chamber was vented and the aluminum foils with CNTs were collected.

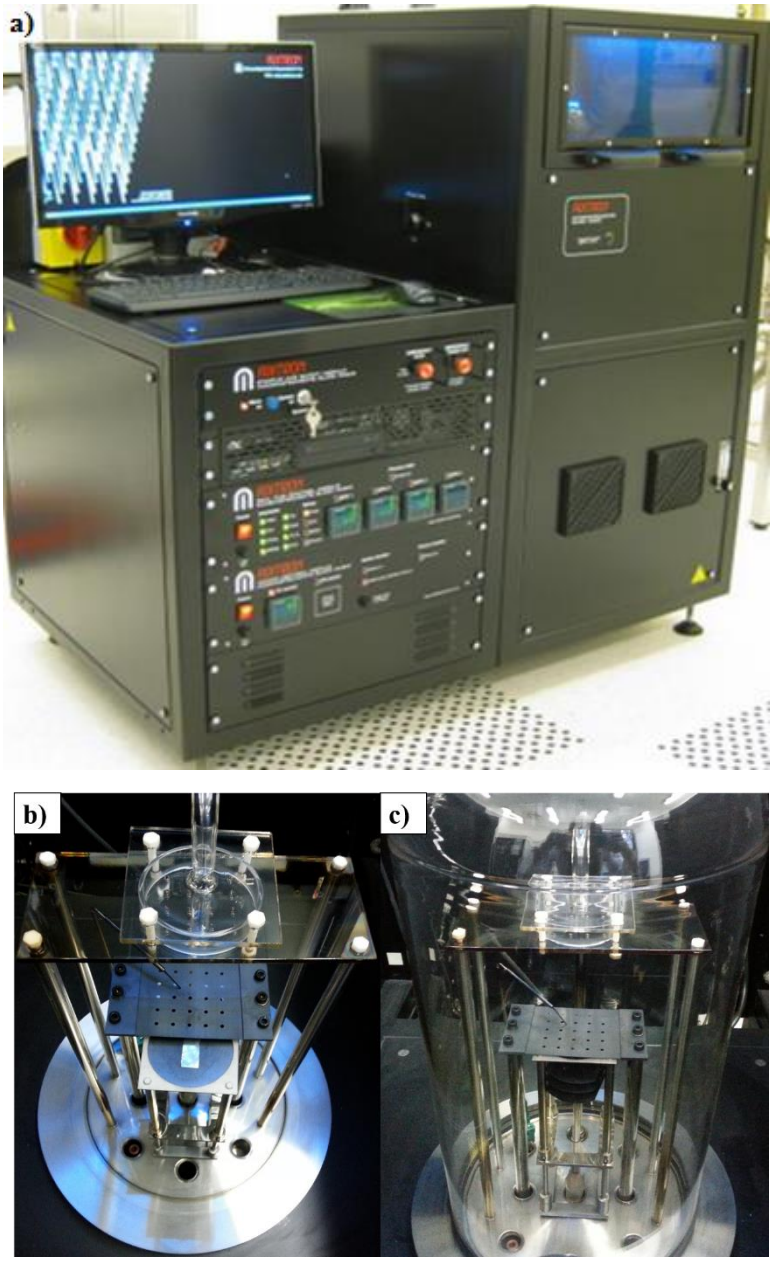

Figure 4.1 Photographs of the (a) CVD system used within the experiments, (b) vacuum chamber without (b) and with (c) the belljar.

With the intention of understanding the effect of catalyst and CVD parameters for the VACNT growth on aluminum foils, a detailed parametric study was conducted. One parameter was changed at a time, while other parameters were kept constant.

4.2 Characterization Methods of CNTs

4.2.1 Scanning Electron Microscopy (SEM)

Morphology of the CNTs was characterized by Nova Nano SEM 430, 10kV field emission scanning electron microscopy. No extra coating was utilized for SEM analysis. Since it is easy to crumple aluminum foil or scratch the CNTs on foil, a piece of the sample was cut and gently attached to SEM mounts using carbon tape.

4.2.2 Transmission Electron Microscopy (TEM)

In transmission electron microscopy, electron beam passes through the CNTs and gives information about the inner structure. For the preparation of TEM samples, VACNTs on aluminum foils were gently scraped off using a scalpel and the obtained powder bits were sonicated with isopropanol. One drop of this solution was drop casted onto lacey carbon coated copper TEM grids. TEM analyses were conducted using a JEOL JEM 2100F scanning/transmission electron microscope operated at 200 kV.

4.2.3 Raman Spectroscopy

In this method, CNT samples were simply exposed to a monochromatic laser (532 nm) in air ambient and scattered laser beams provided information about the structure of the CNTs and defects present within the CNTs. Raman spectroscopy was used as a

fast and nondestructive characterization method for CNTs. A Horiba Jobin Yvon Raman system was used for this purpose.

Within this method, vibrational frequencies that is characteristic of atom and bond structure is monitored. Accordingly, bond structures or defects are distinguishable. For instance, in Raman shifts, 150-350 cm^{-1}signals called as radial breathing modes (RBM) indicate presence of SWNTs, while 1250-1450 cm^{-1} interval named as D band show crystal defects and 1525-1700 cm^{-1} interval, called as G band, is the result of graphitic structure.

4.2.4 Brunauer-Emmett-Teller (BET) Analysis

To examine the specific surface area of the CNT samples, they were subjected to gas molecules that would get adsorbed on the surface of the specimens. By this method, the porosity and surface area of the CNTs were determined. AUTOSORB-6B was used for the analysis.

4.2.5 X-Ray Photoelectron Spectroscopy (XPS)

XPS is a surface sensitive and quantitative technique, which is generally used to precisely measure the elemental composition and chemical state of the materials. In XPS analysis, upon X-Ray irradiation of materials, kinetic energy and the number of electrons that escape from the top most layers of the specimens are simultaneously analyzed. From the kinetic energy, one would get the binding energy values, which are characteristic of elements. A monochromatic Al Ka X-ray source (1486.6 eV) was used for XPS analysis at a base pressure of 10^{-6} Torr with a PHI 5000 VersaProbe. Nominal binding energy of the C 1s was 284.5 eV.

4.3 Fabrication of Supercapacitors

With the intention of the development of supercapacitor electrodes, VACNTs grown on aluminum foils were used in electrochemical measurements. To be able to compare the electrodes accurately, every electrode sample was prepared in the same size; 2.5 cm × 1 cm, where a 0.5 cm^2 edge part of the foil remained empty for contact attachment, as shown in the photograph provided in Figure 4.2. To prevent CNT growth at one edge of the foils, polyimide (kapton) tapes were used to mask that particular area during catalyst deposition. For electrochemical measurements, aqueous 1 M sodium sulfate (Na_2SO_4) solution was used as the electrolyte.

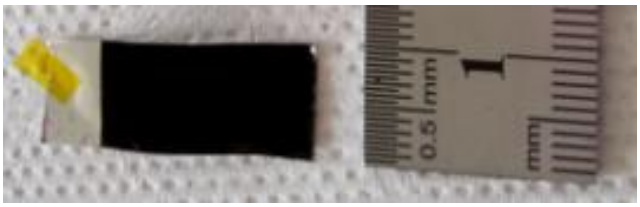

Figure 4.2 Photograph of a CNT/aluminum foil electrode sample.

4.4 Characterization of Supercapacitors

For the electrochemical measurements of the VACNT/aluminum foil electrodes, Gamry 3000 potentiostat/galvanostat system was operated in a three-electrode configuration. All the measurements were related to the interaction of electrode and electrolyte that is encountered at their interface. In the measurement setup, there are working, reference and counter electrodes immersed in an electrolyte solution and these completes a current path for measurements as schematically demonstrated in Figure 4.3. There is also a working sense, attached to the working electrode.

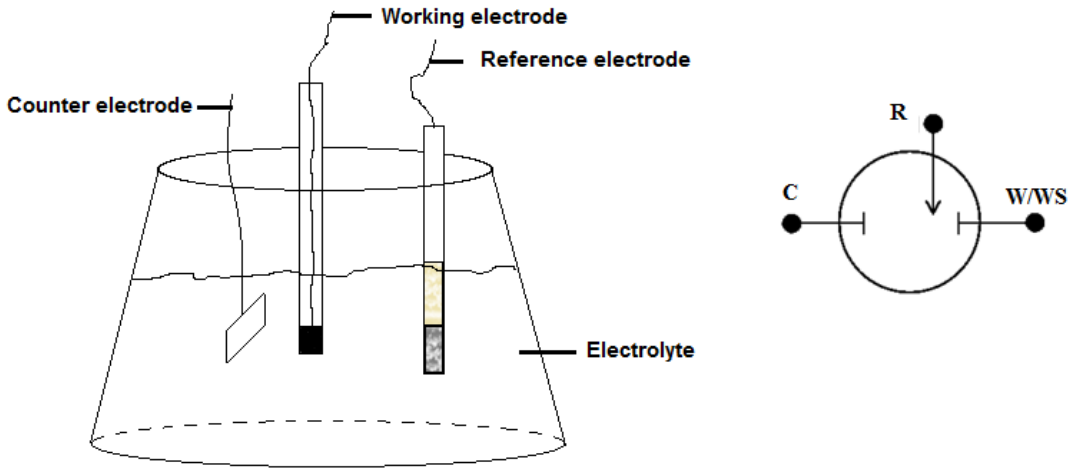

Figure 4.3 Schematic demonstration of a three-electrode cell used in the measurements [69] [70].

The working electrode is the VACNT/aluminum foil sample. Aluminum foil is used as the current collector. Each VACNT act as a parallel capacitive element contributing to the overall capacitance. The surface area of the counter electrode should be bigger than or at least equal to that of the working electrode, so then the complementary charges will be equally distributed and the results show the capacitance of the working electrode. In this set-up, platinum foil was utilized as the counter electrode. Finally, there is a reference electrode with a well-known potential, which was kept constant during the measurements. That was assured by a saturated concentration, where the current flow was almost zero. In this experiment, silver/silver chloride (Ag/AgCl) reference electrode was used that is filled with saturated potassium chloride (KCl). A photograph of the set-up and electrodes is provided in Figure 4.4.

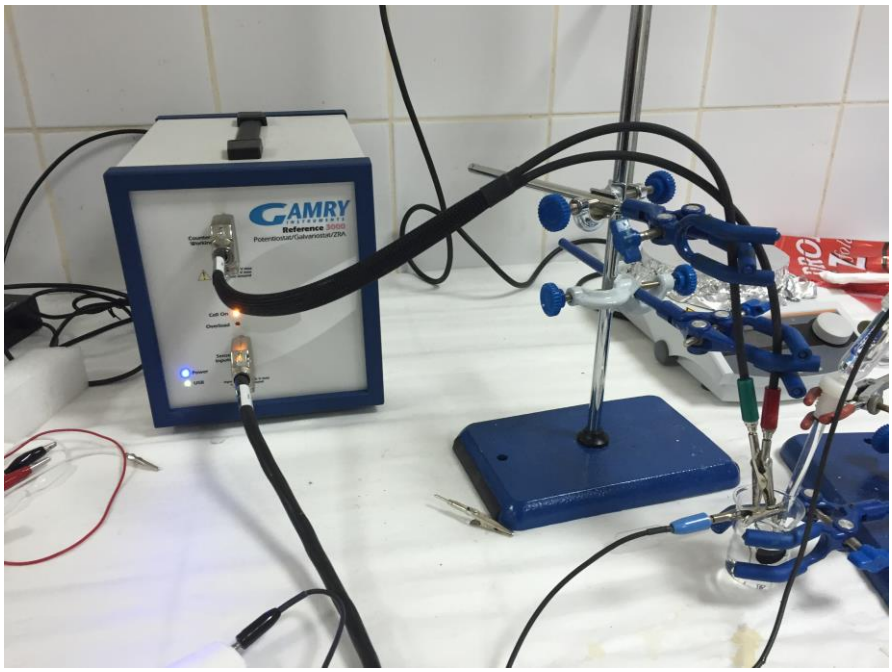

Figure 4.4 Photograph of the experimental set-up utilized in the electrochemical measurements.

In this three-electrode cell set-up, charge flows were between the VACNT/aluminum foil electrode and the platinum foil electrode. On the other hand, measurements were conducted between the working sense and reference electrode [70].

CHAPTER 5

RESULTS AND DISCUSSION

5.1 Parametric Study on CNT Based Electrode Synthesis

To investigate the effects of growth parameters in detail, all the parameters except the one under investigation were kept constant.

5.1.1 Effect of Catalyst and Substrate

Catalyst thickness plays an important role on the CNT growth. When the catalyst thickness was below a threshold value CNTs rarely form on the aluminum foil, as shown in the SEM image provided in Figure 5.1 (a). It was also probable that metal nanoparticles may diffuse towards the substrate during ramping within the CVD process if they are tiny. On the other hand, when the catalyst thickness was higher than an optimum value, CNTs with larger radii form as shown in the SEM image provided in Figure 5.1 (b).

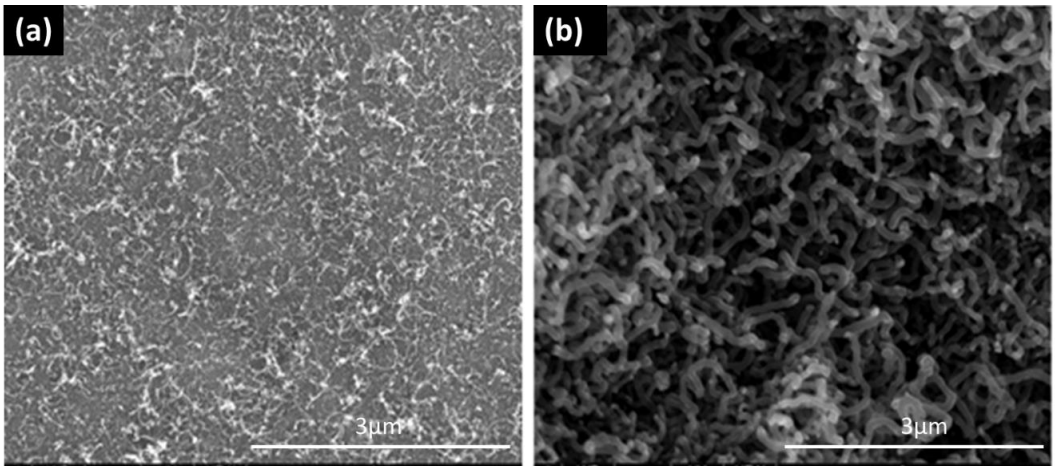

Figure 5.1 SEM images of the CNTs grown using a (a) thin and (b) thick catalyst layer.

With the purpose of evaluating the effect of catalyst deposition methods and substrate types, two pure aluminum foil samples and two kitchen aluminum foil samples were used for the CNT growth. One of the pure aluminum foils and one of the kitchen foils were deposited through USP, while the other two were deposited through PVD.

Photographs of the resulting catalyst deposited samples and the appearance of foils following CNT growth are shown in Figure 5.2. As described earlier, 2.5 cm x 1 cm foil pieces were cut, where one of the edges of the foils was deliberately (with an area of 0.5 cm^2) left empty. The same CVD recipe was used for all the samples.

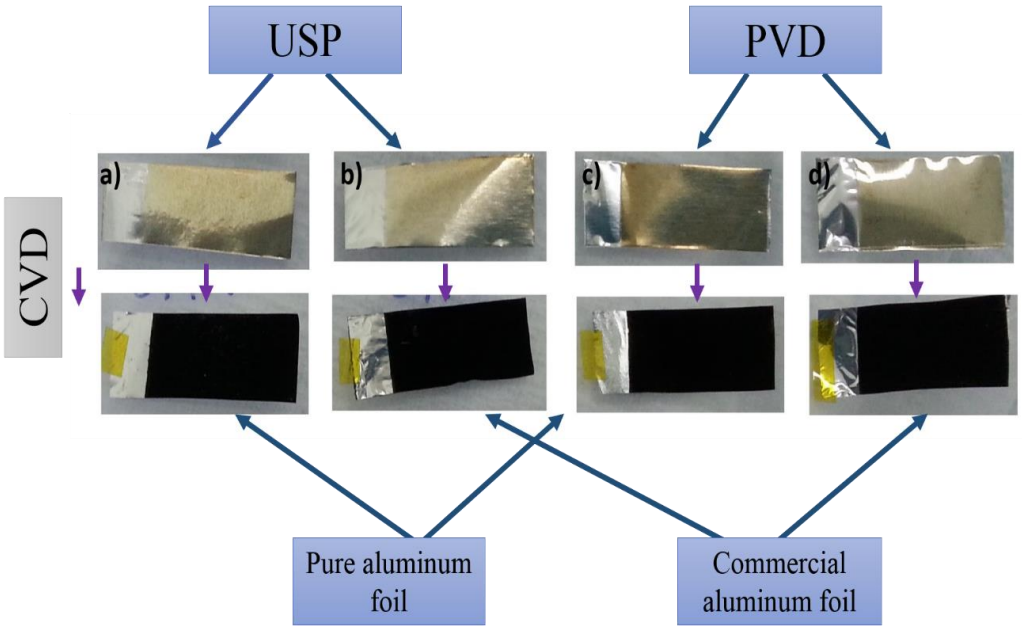

Figure 5.2 Photographs of (a) pure aluminum foil deposited via USP, (b) kitchen aluminum foil deposited via USP, (c) pure aluminum foil deposited via PVD and (d) kitchen aluminum foil deposited via PVD.

These equally sized four samples were positioned one by one within the CVD system and CNTs were grown on these foils under identical conditions. For CNT growth, first the chamber was vacuumed down to 0.1 mbar and then the pressure was set to 8 mbar and kept constant during the entire process. 300 sccm H_2 gas was introduced to the system and kept the same during the entire process. Temperature was then ramped to 600°C at a rate of 200°C/min. Samples were annealed at this temperature for 2 minutes. At the end of the annealing process, the precursor gas, C_2H_2 was introduced into the system at a flow rate of 20 sccm, which initiated the CNT growth. At this stage, temperature was raised to 620°C with a heating rate of 25°C/min. At this temperature, the growth lasted for 5 minutes. At the end of the growth H_2 and C_2H_2 flows were stopped and the chamber was cooled by means of N_2 flow (1000 sccm). Samples were collected following venting. The process parameters were plotted and provided in

Figure 5.3. The right side of the graph shows the changes in gas concentrations with time, while the left side displays the changes in temperature and pressure during the process.

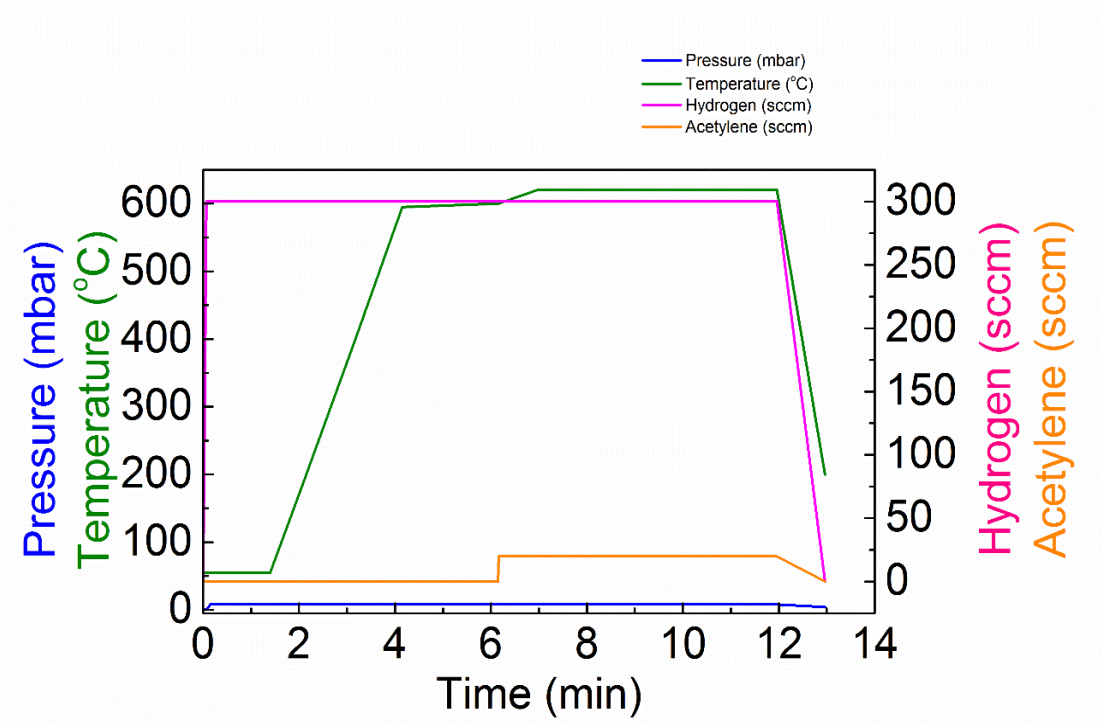

Figure 5.3 Graphs showing the changes in H_2 and C_2H_2 concentrations (right axis) and changes in pressure and temperature with time (left axis).

SEM images of these four samples are provided in Figure 5.4. Top view SEM images of pure aluminum foil, catalyst deposited via USP, commercial aluminum foil, catalyst deposited via USP, pure aluminum foil, catalyst deposited via PVD and commercial aluminum foil, catalyst deposited by PVD samples are shown in Figures 5.4 (a),(c),(e),(g). Figure 5.4 (b),(d),(f) and (h) shows the corresponding cross-sectional SEM images.

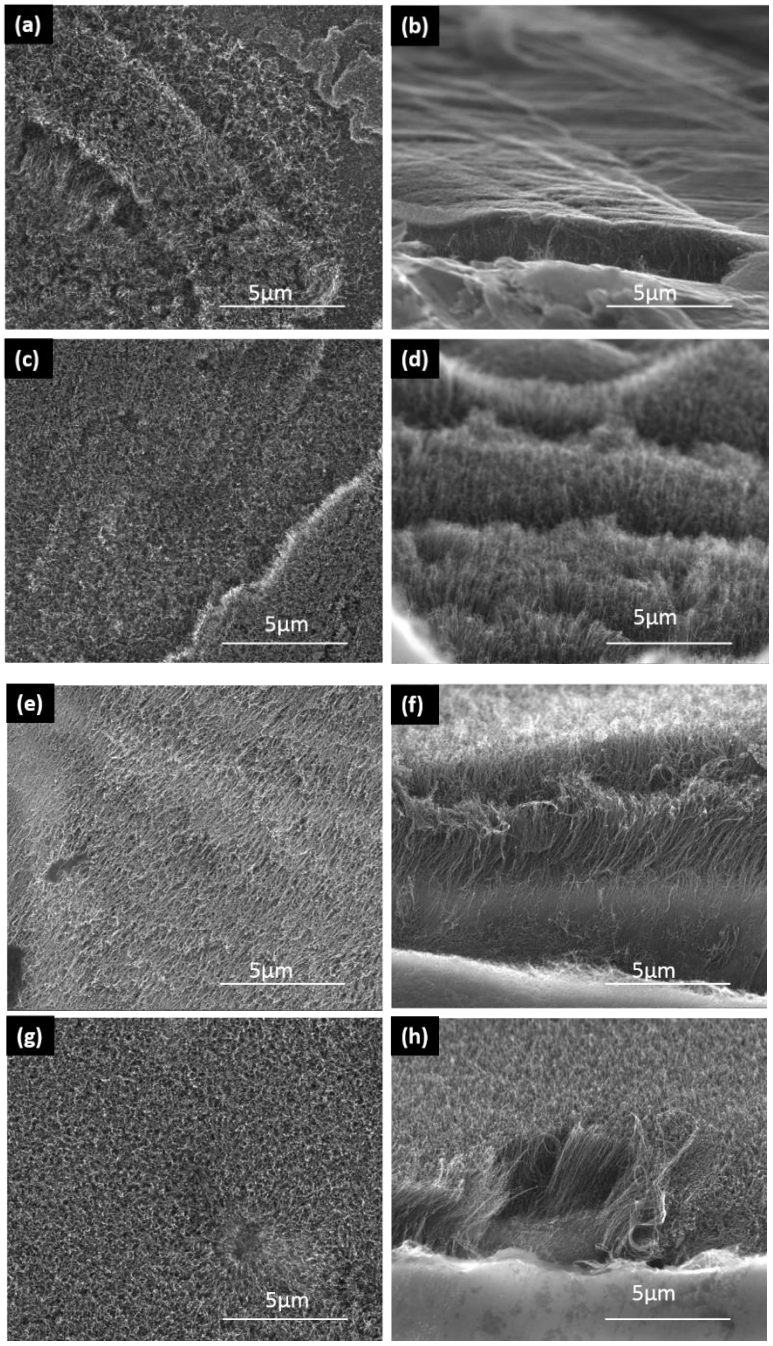

Figure 5.4 (a) Top-view, (b) cross-sectional SEM image of pure aluminum foil, catalyst deposited via USP (c) top-view, (d) cross-sectional SEM image of kitchen aluminum foil, catalyst deposited via USP (e) top-view, (f) cross-sectional SEM image of pure aluminum foil, catalyst deposited via PVD (g) top-view, (h) cross-sectional SEM image of kitchen aluminum foil, catalyst deposited via PVD.

Although the CNTs grown on pure aluminum foils seemed denser, all samples had similar results with respect to the length and alignment of the CNTs. The thickness of pure aluminum foil was 0.025 mm, while that of the kitchen aluminum foil was about 0.018 mm. It was anticipated that the thick pure aluminum foil withstands more to the CNT growth temperatures, resulting in a denser VACNT growth. To determine the surface area of the samples, the BET analysis were performed, results of which can be seen in Table 5.1.

Table 5.1 BET analysis results for the CNTs grown on different substrates using different catalysts.

Sample	**Specific Surface Area (m^2/g)**
Pure aluminum foil, catalyst deposition via USP	39.99
Kitchen aluminum foil, catalyst deposition via USP	135.5
Pure aluminum foil, catalyst deposition via PVD	19.4
Kitchen aluminum foil, catalyst deposition via PVD	58.77

A significant difference of BET surface area for samples can be seen. Although the SEM images of samples seem similar in Figure 5.4, the specific surface area also depends on number of walls that we cannot decide from SEM images. Raman spectra for these four samples are provided in Figure 5.5.

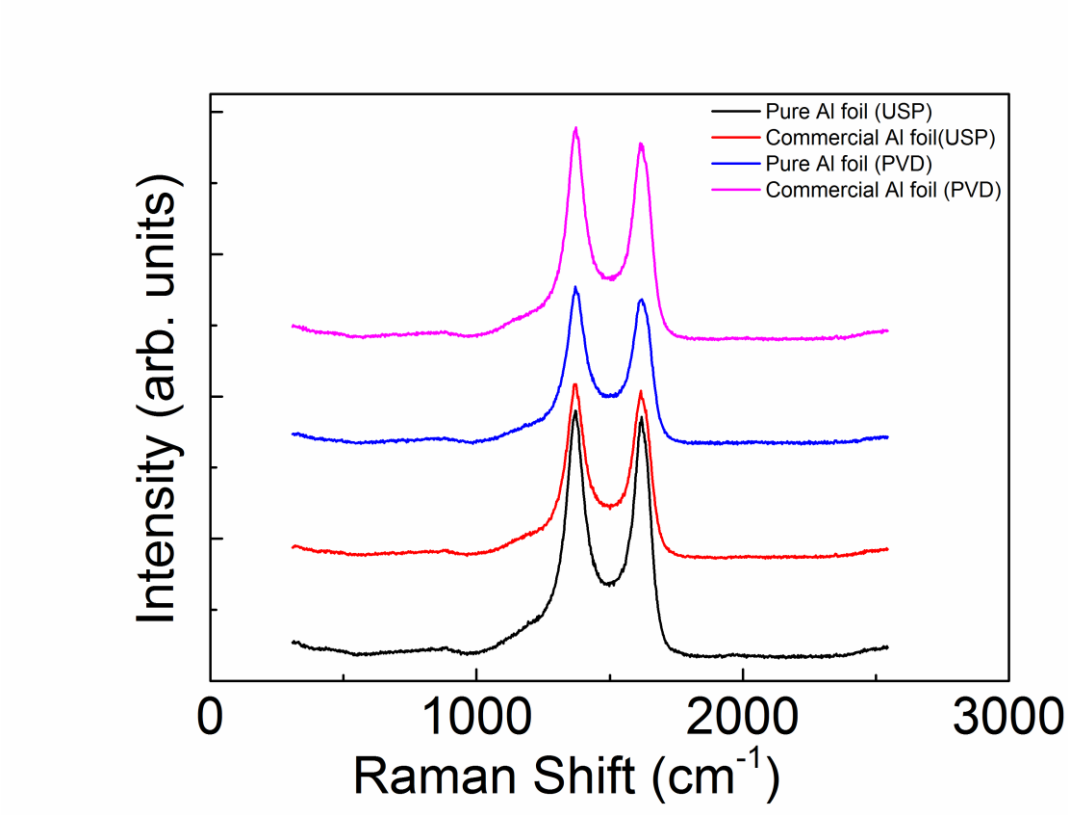

Figure 5.5 Raman spectra for CNTs grown on different substrates using different catalysts.

The ratio of the intensities of the D band to G band can be used to evaluate the purity, defect concentrations and relative amount of amorphous carbon within the samples. The I_D/I_G ratios were found to be similar for these four samples, indicating that the catalyst deposition route and the type of the substrate has almost no influence on the CNT properties. Since there were no signals within the 150-350 cm^{-1} range, synthesized CNTs were multi walled. To examine the multiwalled structure in detail, one of the samples were investigated by TEM. Low and high resolution TEM images are provided in Figure 5.6 (a) and (b), respectively. TEM analysis revealed that the obtained CNTs were few walled (2 - 8 sidewalls) and defective in nature, which is in agreement with the Raman results.

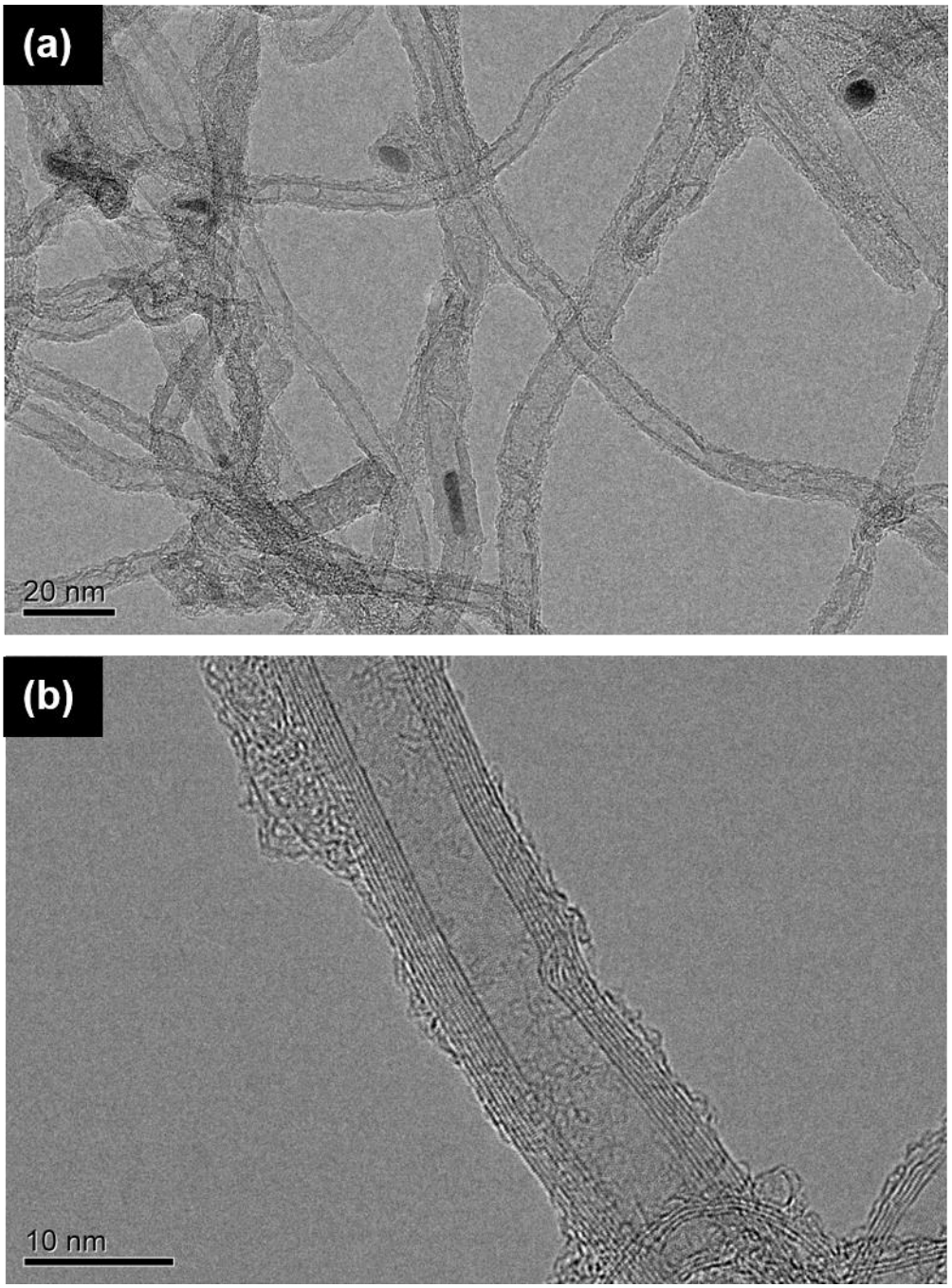

Figure 5.6 (a) Low-resolution and (b) high-resolution TEM images of synthesized MWNTs.

5.1.2 Effect of Temperature

Temperature imposes a constraint on the CVD growth of CNTs on aluminum foil. It is because the growth takes place at temperatures that are very close to the melting point of aluminum. High temperatures are necessary for the efficient dissociation of the source gas; however, it has to be lower than the melting temperature of the foils. As the temperature increases, gases accelerate and the reaction rate increases resulting in the synthesis of longer CNTs [39]. It is advantageous to find the maximum growth temperature. Although identical substrates were used in this work, melting point of the substrates did change with respect to the growth pressure, which was also related with the amount of gases within the chamber.

For each catalyst type, the first step in CVD is to find a suitable recipe that results in the formation of the darkest CNT layer on aluminum foils.

For the growth, the foil samples were exposed to different growth temperatures above the annealing temperature. Growth temperatures were increased stepwise with 10°C intervals until the substrates start to melt or degrade. All the other parameters were kept constant. The annealing temperature of the recipe was 600°C; so in the first trial the carbon precursors were introduced into the chamber right after the annealing process and temperature was kept constant during the growth process. In the second, third and fourth trials, the growth temperatures were adjusted as 610, 620 and 630°C, respectively. Noticeably, higher growth temperatures resulted in the formation of darker samples. The foil started to get damaged during the 640°C growth. Although the foil recovered from this trial was very black as compared to others grown at lower temperatures, it was crumpled and could easily break into pieces. Therefore, these pieces cannot be used as electrodes. This maximum temperature depends on complex and synergistic parameters such as pressure, thickness as well as the type of both the catalyst and the substrate and reactions occur during the CNT growth. The temperature was then decreased in steps of 5°C in order to find the maximum temperature at which the foil remained intact. 635°C growth locally melted and damaged the substrate. The

substrate survived during 630°C growth; but, the color of the backside of the substrates changed, showing that the substrates were still getting effected at this temperature. Figure 5.7 shows top-view and cross-sectional SEM images of the samples grown at temperatures of 600, 610, 620 and 630°C.

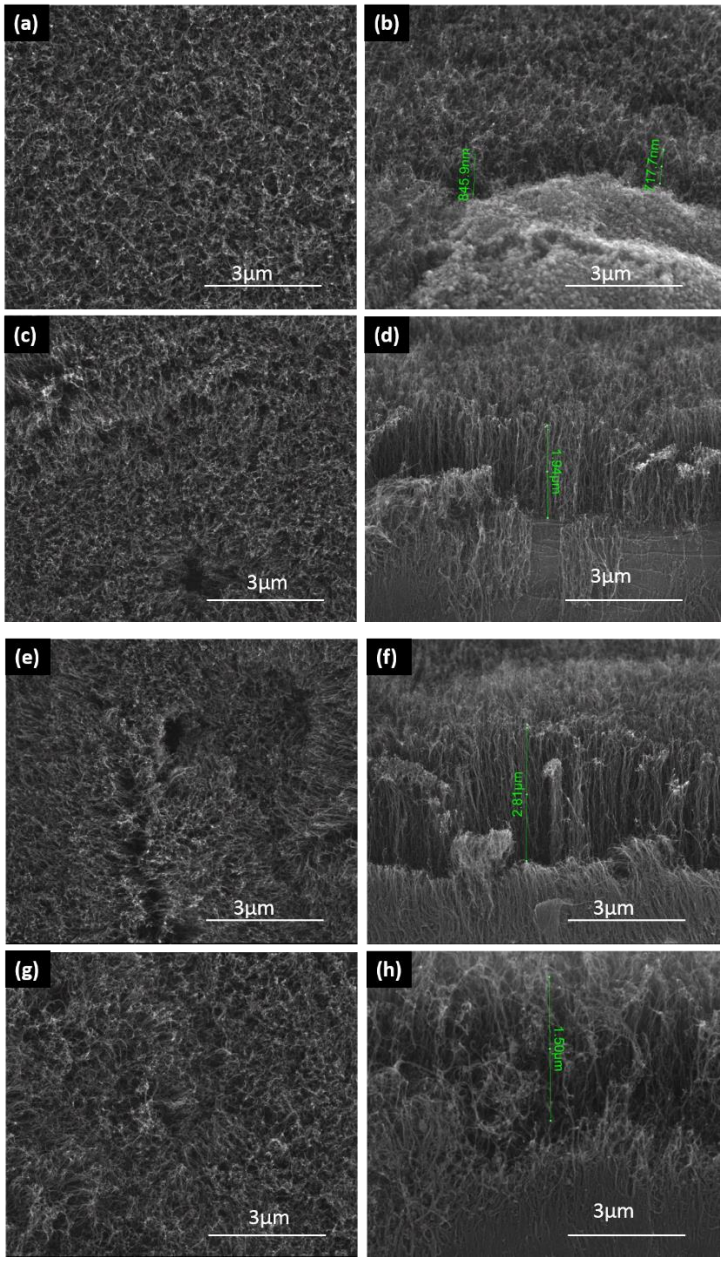

Figure 5.7 (a) Top-view and (b) cross-sectional SEM image of CNTs grown at 600°C, (c) top-view and (d) cross-sectional SEM image of CNTs grown at 610°C, (e) top-view and (f) cross-sectional SEM image of CNTs grown at 620° C, (g) top-view and (h) cross-sectional SEM image of CNTs grown at 630°C.

It is apparent that the length of the CNTs increases with temperature. In addition, their alignment gets improved. However, for the sample grown at 630°C (Figure 5 (g) and (h)), due to the damage given to the foil, CNTs were short, entangled and a bit curly. Their vertical alignment was partially destroyed. CNTs could possibly get submerged to the substrate when the substrate is in quasi-liquid state or the accelerated gas mixtures etch or curve the CNTs. The length of the CNTs with respect to the growth temperature is plotted in Figure 5.8.

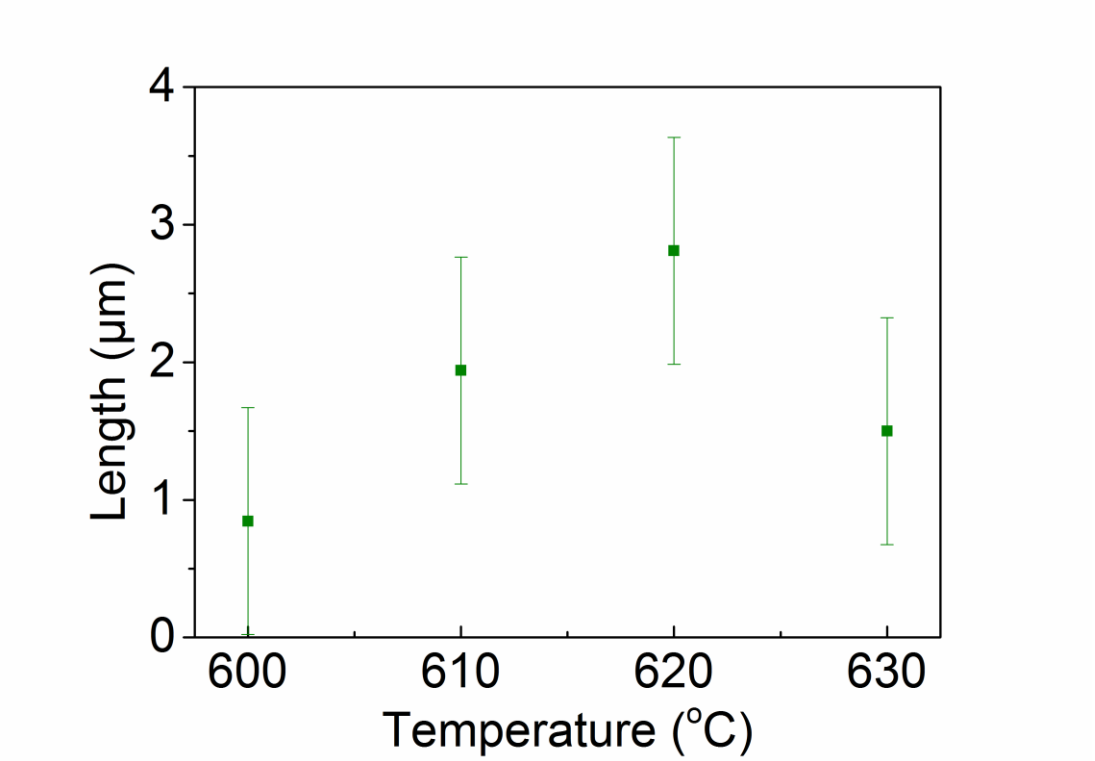

Figure 5.8 The length of CNTs as a function of growth temperature.

The Raman spectra of samples that were grown at temperatures of 600, 610, 620 and 630°C are shown in Figure 5.9 (a)-(d), respectively.

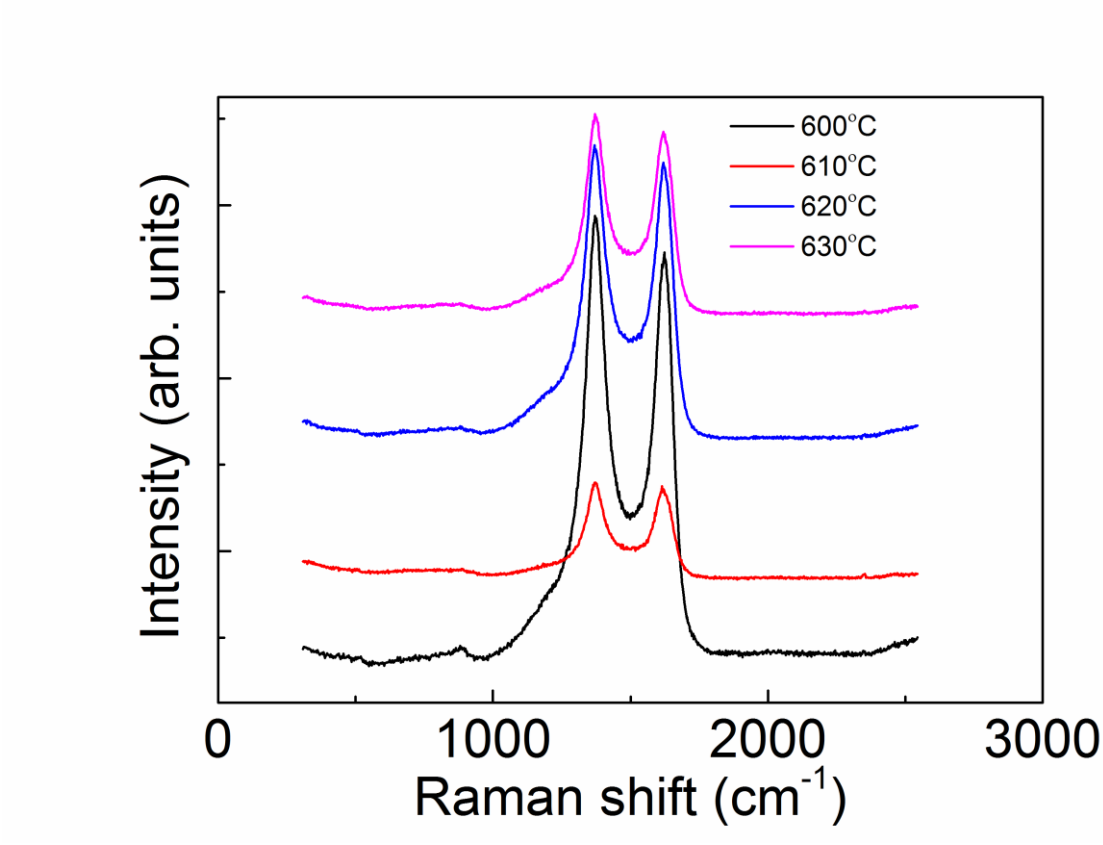

Figure 5.9 Raman spectra of the samples grown at different temperatures.

Similar to the results obtained for different catalyst types, I_D/I_G ratios were found to be almost the same for the CNTs grown at different temperatures. This was not an unexpected result as the substrate pieces were cut from the same catalyst sample and all the parameters except temperature were identical. Subsequent to the completion of the annealing process, the growth temperatures were attained and the growth lasted for 5 minutes. Therefore, in principal, increasing the growth temperature also increases the total growth time.

5.1.3 Effect of Pressure

Computer controlled CVD system allowed easy control over the growth pressure. As the pressure decreases, mean free path of the gases increase resulting in the reduction of their diffusivity. Inversely, when the pressure increases a lot, the diffusivity of the gases might get too high, they could pass beyond the catalyst without reacting with it, preventing the CNT synthesis. That is to say, there is an optimum pressure for the synthesis of dense VACNTs.

In this part of the study, 20 nm aluminum and 2.6 nm iron layers were deposited by PVD onto pure aluminum foil substrates. Aluminum and iron depositions were carried out on alternate days to convert the aluminum support layer to aluminum oxide through the air exposure of the sample. To complete catalyst deposition, the samples are inserted in oven at 500°C for one hour to anneal them. To analyze the oxidized catalyst layers, XPS analysis was performed before and after the annealing process. The XPS spectra of the not annealed sample is shown in Figure 5.10.

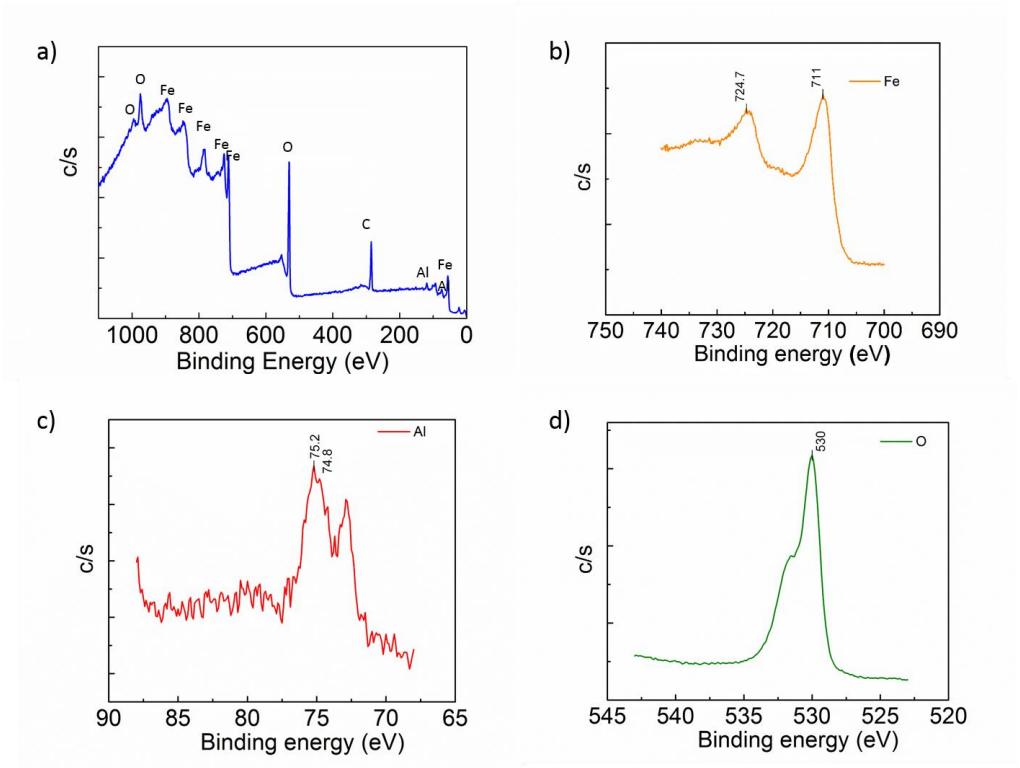

Figure 5.10 XPS of catalyst (a) general, (b) iron, (c) aluminum and (d) oxygen scanning before annealing process.

In Figure 13 (a), aluminum, iron and oxygen peaks are observable as expected. Moreover, this result illustrates there are no contamination during the evaporation process. In the iron peak graph in Figure 13 (b) the peaks at 724.4 and 711 eV are the results of Fe_2O_3 while the aluminum graph in Figure 13 (c) has the peaks of Al_2O_3 at 74.5 and 76.5. It is also apparent that when the foils are waited in air environment during a day, they are oxidized. The oxygen peaks in 527.7 and 530.6 eV interval in Figure 13 (d) also verify that the sample is oxidized. The XPS result of the annealed catalyst sample is shown in Figure 5.11.

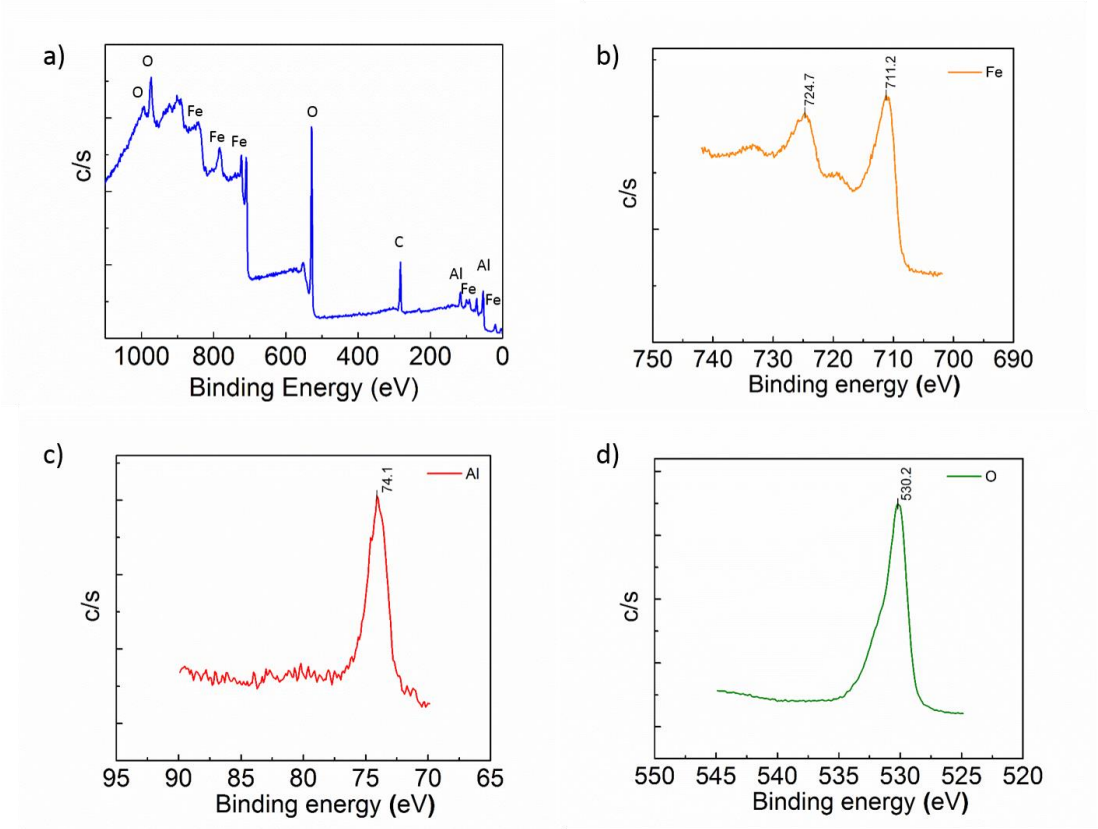

Figure 5.11 XPS of catalyst (a) general, (b) iron, (c) aluminum and (d) oxygen scanning after annealing process.

XPS results of the two samples show that peaks are in range before and after annealing process. It is clear that the results are comparable with Figure 5.10. There are no unexpected peaks after annealing process. These results also show that annealing process do not contaminate the samples. The only observable difference is in Figure 5.11 (c), where there is an additional peak at Al_2O_3 at 74,1 eV.

As indicated before, foils with the same size were used and the optimum growth recipe was determined first from the dark appearance of the foils right after the growth. As last, the effect of pressure on the CNT growth was investigated. For this, the regulated pressure was kept constant from the beginning to the end of the CVD process. A

mechanical pump in conjunction with a computer controlled pneumatic valve were used to prevent the pressure changes inside the chamber. This is because the pressure gets affected when a gas is introduced into the chamber or a gas is cut. The gas flow rates were determined as 300 and 20 sccm for H_2 and C_2H_2, respectively. Then the growths were performed, using pressure values of 8, 10, 15, 50 and 80 mbars. The photographs of the samples following CVD process are provided in Figure 5.12.

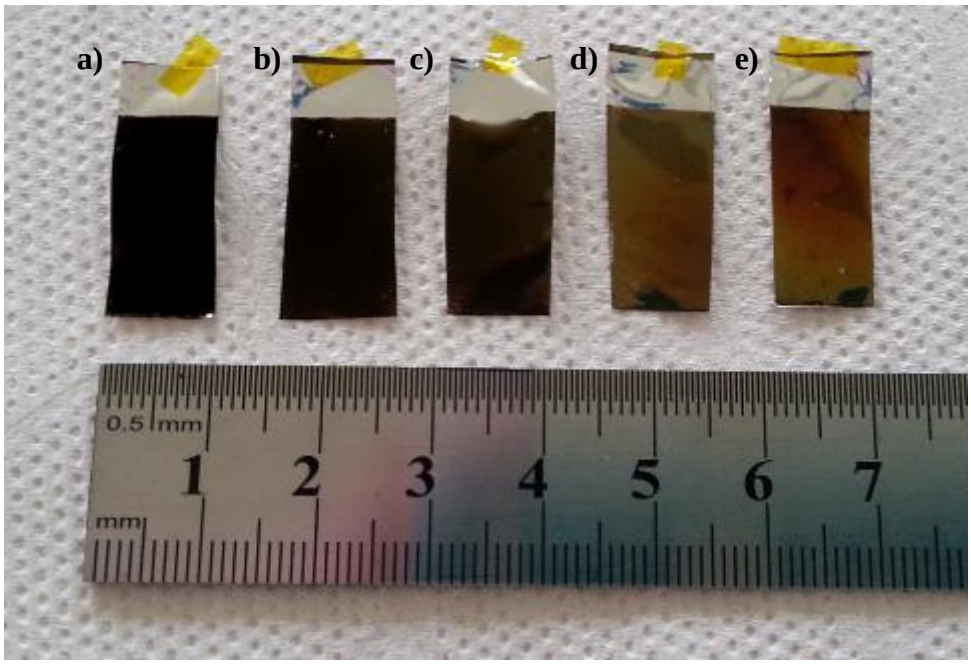

Figure 5.12 Photographs of the pure aluminum foils following CVD growth, using pressure values of (a) 8, (b) 10, (c) 15, (d) 50 and (e) 80 mbars.

It is clear for this catalyst and recipe that an increase in the growth pressure decreases the CNT growth. As the number, length or verticality of the CNTs decrease, the absorbance of light decreases resulting in lighter substrate colors. Moreover, since the used substrate is shiny, reflectance increases as larger substrate layers become visible

between rare CNTs. These samples were also investigated by Raman spectroscopy and the results are provided in Figure 5.13.

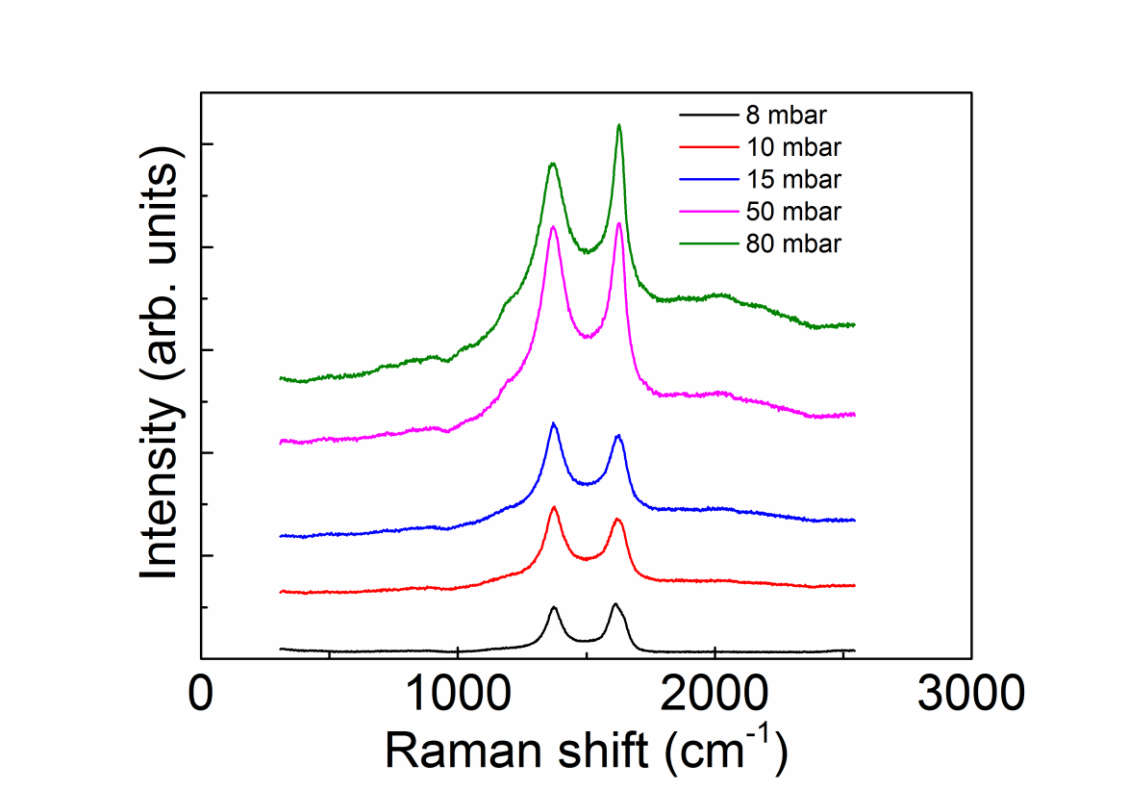

Figure 5.13 Raman spectra of the CNTs grown using different pressure values.

In this recipe, I_D/I_G ratio was higher than 1 for CNTs grown at pressures of 8, 10 and 15 mbars. On the other hand, as the pressure gets higher, this ratio gets smaller than 1, as seen in Figures 5.13. Increasing the pressure increases the gas flow rates, leading to the formation of less defected CNTs. This could be attributed to increased collision probabilities of the gases and catalytic nanoparticles. In addition, high growth pressures decrease the effect of heat damage since heat is dispersed along higher number of gas molecules. Another deduction from Raman results is that the I_D/I_G ratio decreases as the pressure increases, while the peak intensities gets enhanced. The

increase in peak intensities is simply due to shiny surfaces of aluminum foils following CVD growth at high pressures.

5.1.4 Effect of Gas Flow Rates

Gas flow rate is another significant parameter in the CNT growth. As mentioned before, if the gases are introduced too slowly to the system, no reaction takes place. In contrast, when they are introduced fast, catalyst poisoning may occur. In such a situation, hydrogen directed towards the catalyst dilutes the precursor and prevents catalyst poisoning by carbon. On the other hand, if hydrogen flow rate is too high, it may etch the freshly formed CNTs. As a result, each catalyst has an optimum gas flow rate for the nucleation of CNTs.

To examine the effect of gas flow rates, 1.7 nm Fe and 13.3 nm Al deposited pure aluminum foil substrates were prepared. Hydrogen flow rate was kept constant during the synthesis. First, the effect of hydrogen flow rate was investigated. For this, acetylene flow rate was set to 20 sccm and all the parameters except the hydrogen flow rate was kept constant. Growth pressure was 8 mbar. Three different experiments were conducted with hydrogen flow rates of 100, 200 and 300 sccm, with corresponding H_2: C_2H_2 ratios of 5:1, 10:1 and 15:1, respectively. The top-view and cross-sectional SEM images of the CNTs grown under different hydrogen gas flow rates are provided in Figure 5.14.

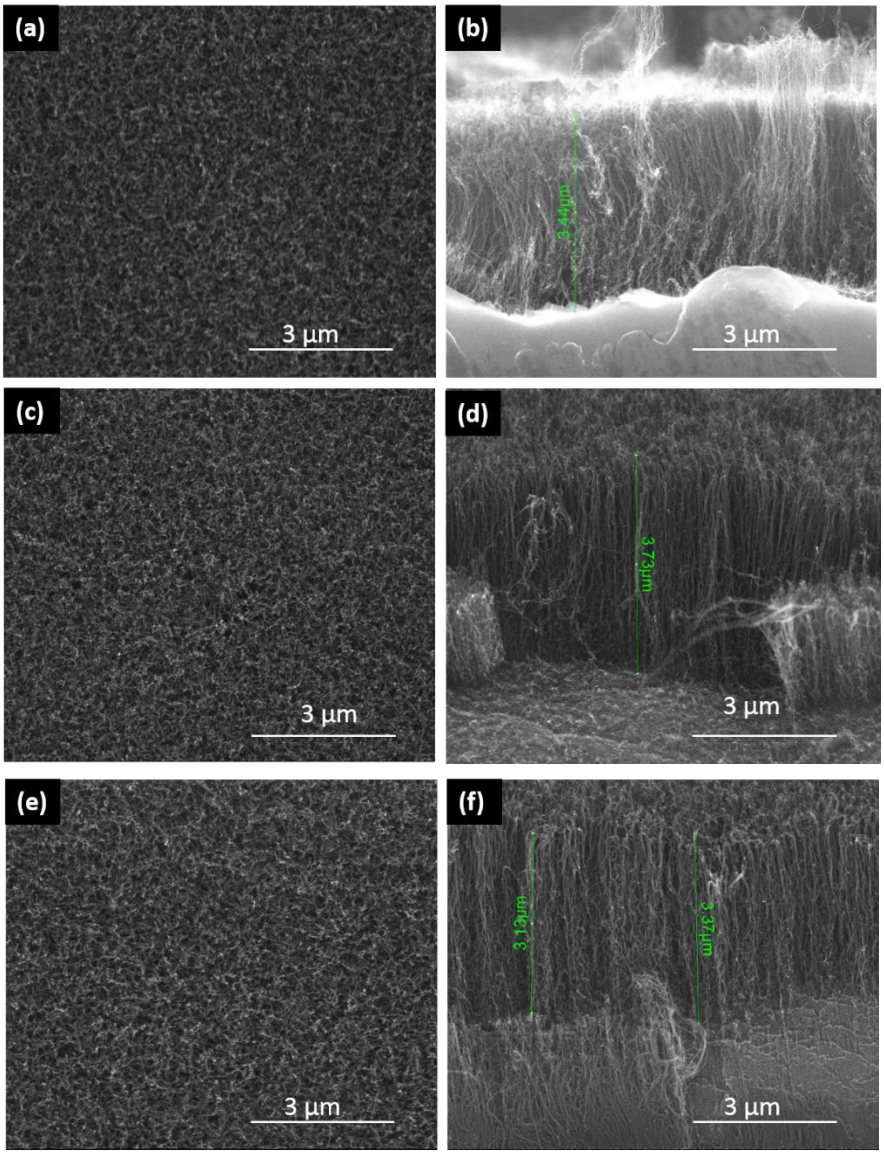

Figure 5.14 (a) Top-view and (b) cross-sectional SEM images of CNTs grown at a H_2: C_2H_2 ratio of 5:1. (c) Top-view and (d) cross-sectional SEM images of CNTs grown at a H_2: C_2H_2 ratio of 10:1. (e) Top-view and (f) cross-sectional SEM images of CNTs grown at a H_2: C_2H_2 ratio of 15:1.

The change in the length of the CNTs with gas flow rates is provided in Figure 5.15. As shown, the change in CNT length is almost insignificant.

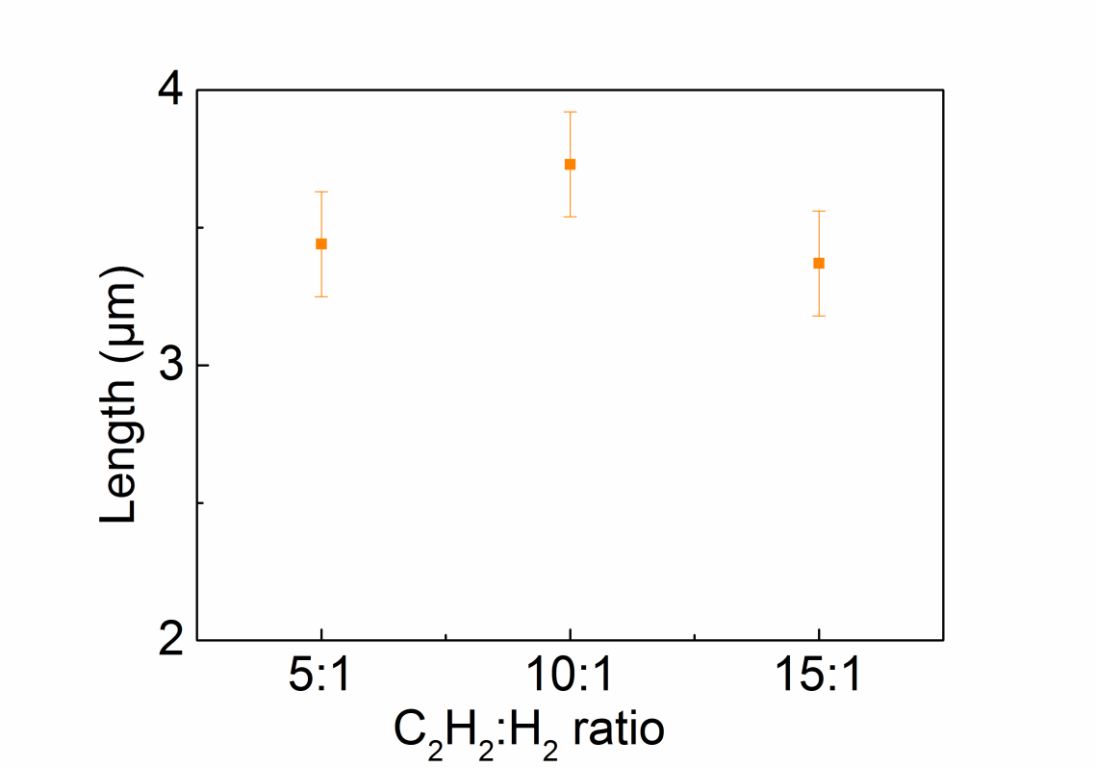

Figure 5.15 The length of CNTs as a function of H_2: C_2H_2 ratio.

It is expected that the density of CNTs decrease with an increase in the hydrogen flow rate. As the ratio of H_2:C_2H_2 increases, it is supposed that the hydrogen dilutes acetylene faster than the optimum rate for CNT nucleation. It is also possible that the excess amount of hydrogen may etch the recently formed CNTs. Although the ratio of flow rates change, the samples were all dense enough for the formation of VACNTs. These samples were also investigated by Raman spectroscopy, results of which are provided in Figure 5.16.

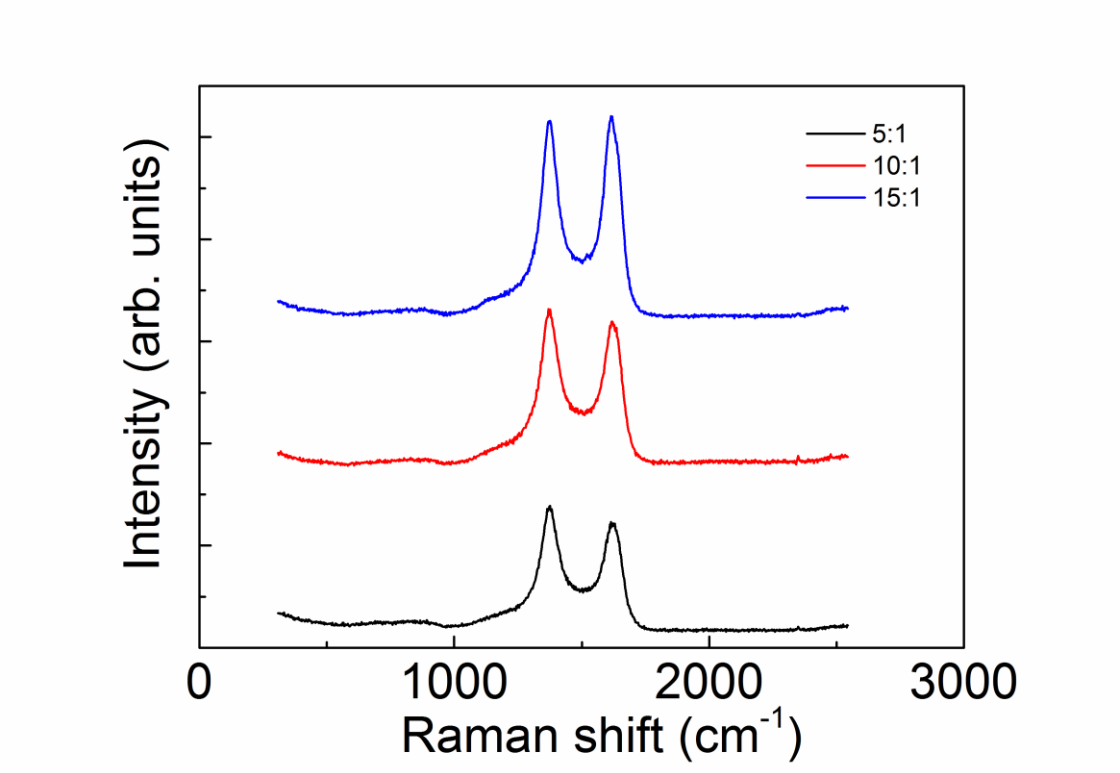

Figure 5.16 Raman spectra of the CNTs grown using different H_2:C_2H_2 ratios, where hydrogen flow rates were kept constant.

With the increase in the amount of hydrogen, I_D/I_G ratio decreases. Since the I_D/I_G ratio for the sample grown using a H_2:C_2H_2 ratio of 15:1 is less than 1, it can be thought that hydrogen is profitable as it decrease the formation of amorphous carbon.

In order to further investigate the effect of gas flow rates, this time the acetylene flow rate was set to 100 sccm and all the parameters except the acetylene flow rate was kept constant. Three different experiments were conducted again with hydrogen flow rates of 100, 200 and 300 sccm, with corresponding H_2: C_2H_2 ratios of 1:1, 2:1 and 3:1, respectively. Growth pressure was 8 mbars again. SEM images of the CNTs grown under different hydrogen gas flow rates are provided in Figure 5.17.

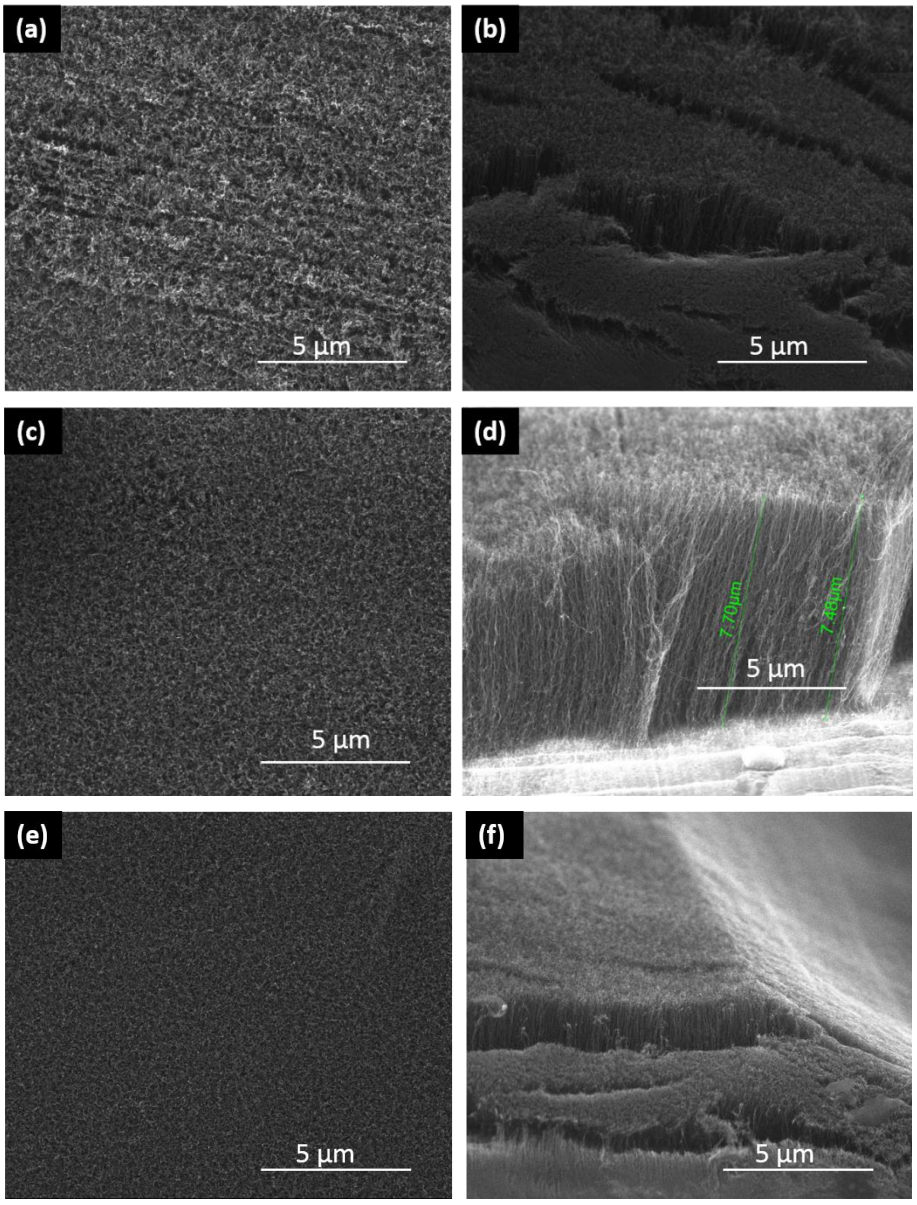

Figure 5.17 (a) Top-view and (b) cross-sectional SEM images of CNTs grown at a H_2: C_2H_2 ratio of 1:1. (c) Top-view and (d) cross-sectional SEM images of CNTs grown at a H_2: C_2H_2 ratio of 2:1. (e) Top-view and (f) cross-sectional SEM images of CNTs grown at a H_2: C_2H_2 ratio of 3:1.

It is realized that, with the adjustment of H_2: C_2H_2 ratio to 1:1, 2:1 and 3:1, the density and length of the VACNTs significantly change from the corresponding values investigated in the first part (Section 5.1.4). In fact, the length of the CNTs was a few times longer (above 7 μm) even though the actual length of the CNTs could not be determined due to bent foil corners. These samples were also analyzed by Raman spectroscopy and the results are provided in Figure 5.18.

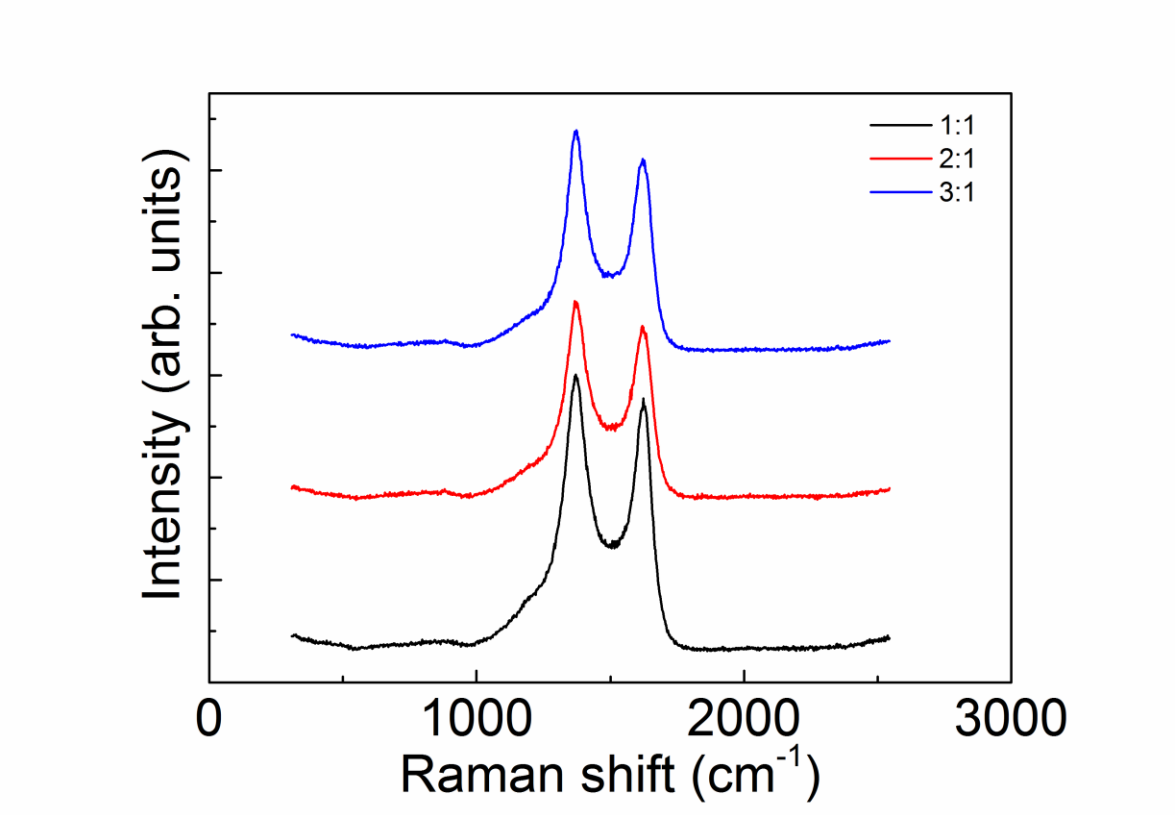

Figure 5.18 Raman spectra of the CNTs grown using different H_2:C_2H_2 ratios, where acetylene flow rates were kept constant.

In this part of the experiments, hydrogen flow rates were close to that of acetylene, and the flow ratios were clearly smaller than the first trial. I_D/I_G ratios were found to

be larger than 1 in contrast to H_2:C_2H_2 ratio of 15:1, as discussed before in Figure 5.16.

5.1.5 Effect of Annealing

In this part, the effect of annealing time and temperature were investigated. Pure aluminum substrates with 1.7 nm Fe and 13.3 Al catalyst were prepared with identical sizes and all parameters except annealing time and temperature (one at a time) were kept constant. All the growth stages till the introduction of carbon precursors affect the transformation of catalyst thin film into nanoparticle form. The hydrogen flow rate and temperature as well as the temperature ramp rate play a critical role on the development of catalyst nanoparticles. The maximum temperature before the acetylene delivery and time that the samples stay at this temperature were examined at this stage. If the temperature was too high or if the samples were kept too long at that temperature, the catalytic metal nanoparticles grow larger in size resulting in the formation of thick CNTs. In the first part of these experiments, annealing temperature was successively adjusted as 500, 550 and 600°C. In addition, the annealing time was determined as 2 minutes for these experiments. Corresponding SEM images from the samples grown with this recipe is shown in Figure 5.19.

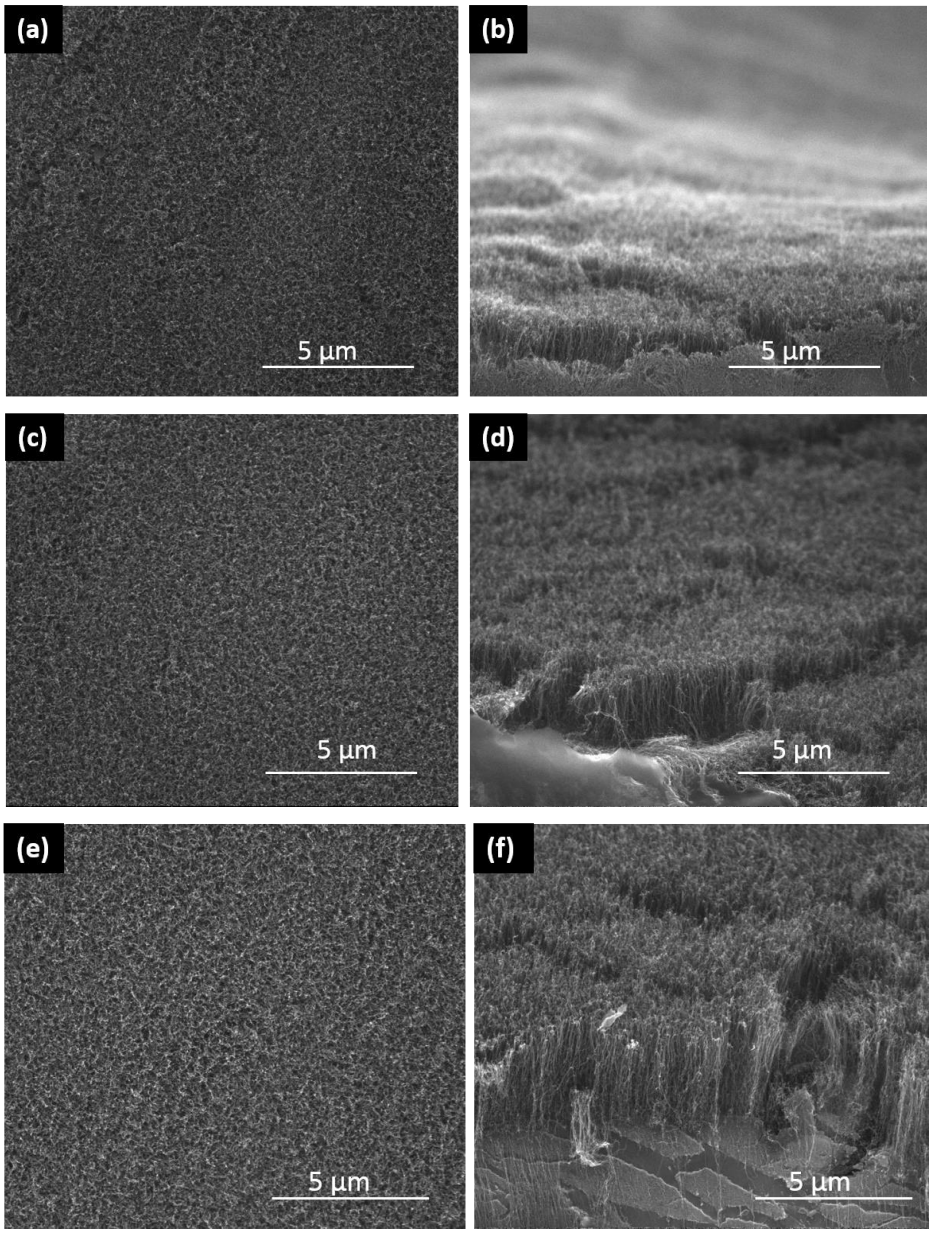

Figure 5.19 (a) Top-view and (b) cross-sectional SEM images of 500°C annealed sample. (c) Top-view and (d) cross-sectional SEM images of 550°C annealed sample. (e) Top-view and (f) cross-sectional SEM images of 600°C annealed sample.

Although different annealing temperatures were used, the resulting SEM images of the samples seemed similar. At the end of the annealing process, acetylene was delivered into the chamber and the temperature was raised to the growth temperature and the growth endured 5 minutes at constant temperature. The decrease in the annealing temperature resulted in an increase in the time to reach the growth temperature. In other words, the total growth time under acetylene flow increased. Raman spectra of these samples are provided in Figure 5.20.

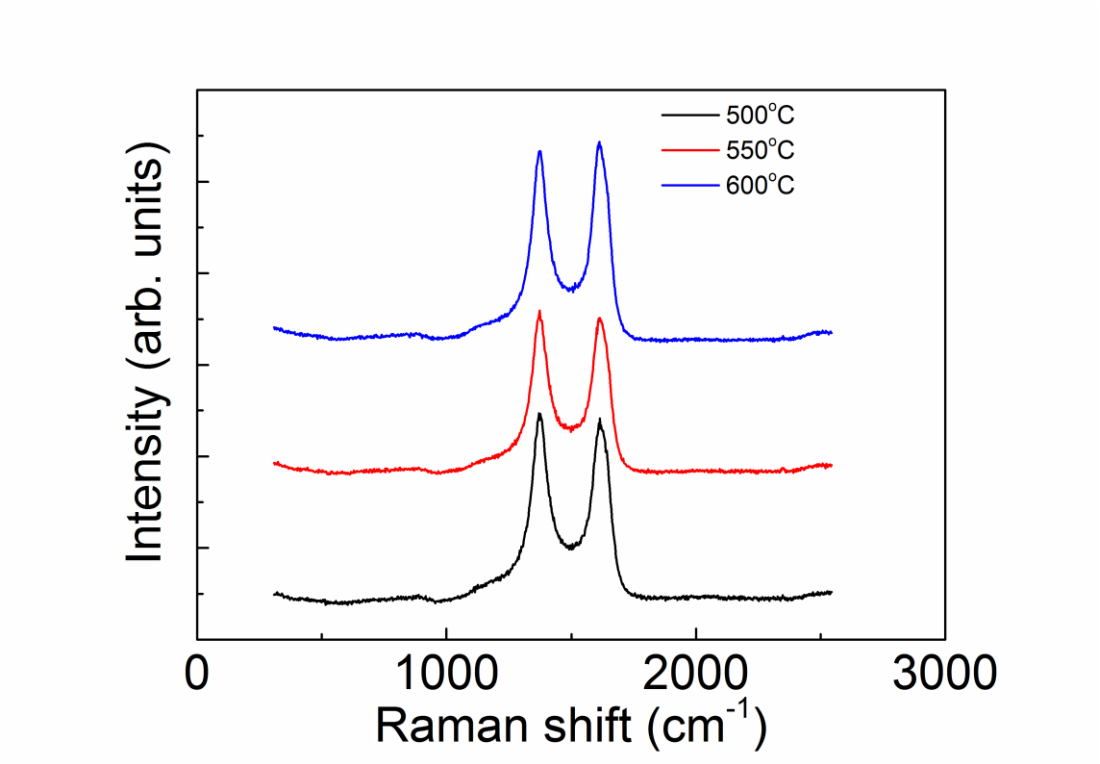

Figure 5.20 Raman spectra of the CNTs grown using different annealing temperatures.

The I_D/I_G ratio was less than 1 for the CNTs grown using an annealing temperature of 600°C, while the other two samples had a I_D/I_G ratio of more than 1. Although the difference between the ratios were not too high, the difference could simply be due to the relatively short exposure time to acetylene gas at higher annealing temperatures.

In the second part of this investigation on the effect of annealing, the annealing temperature was fixed to 600°C and the effect of annealing time was investigated. CNTs were grown using annealing times of 1, 2, 4 and 8 minutes. Corresponding SEM images from the samples grown with different annealing times are shown in Figure 5.21 (a) - (h).

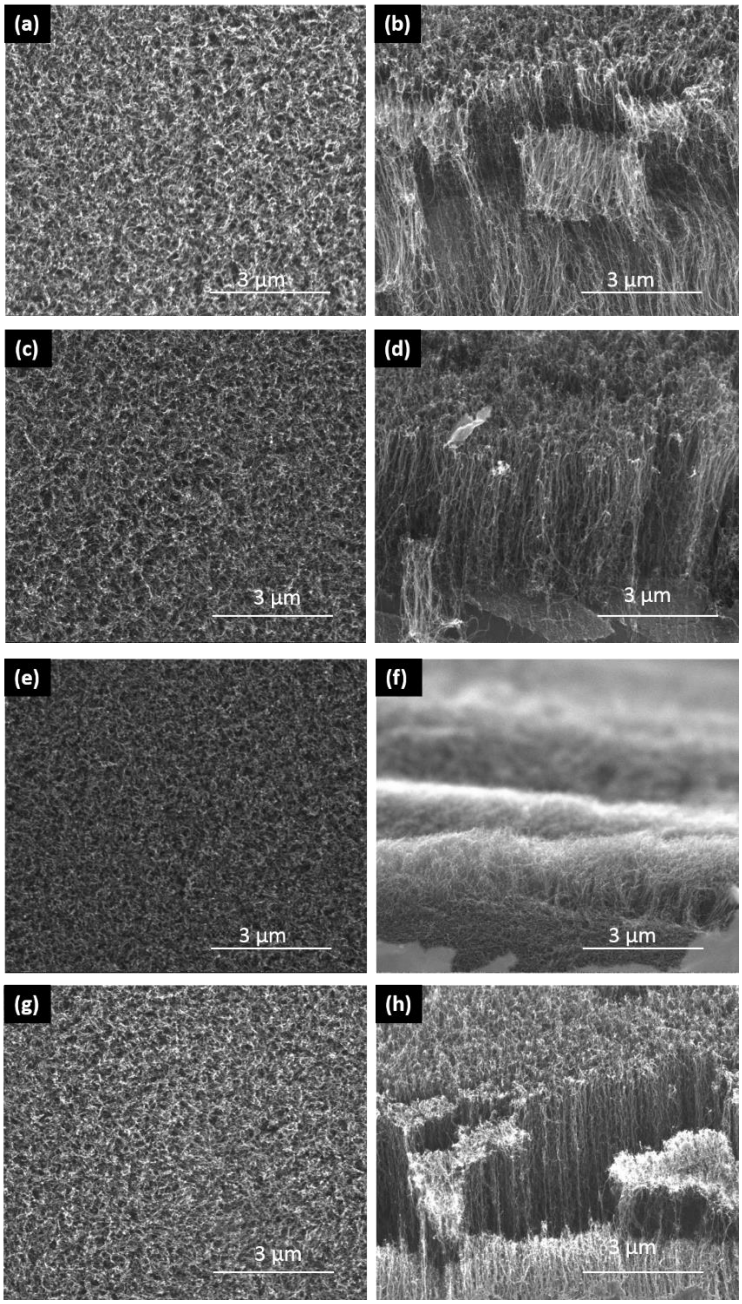

Figure 5.21 (a) Top-view and (b) cross-sectional SEM images of 1 minute annealed sample. (c) Top-view and (d) cross-sectional SEM images of 2 minutes annealed sample. (e) Top-view and (f) cross-sectional SEM images of 4 minutes annealed sample. (g) Top-view and (h) cross-sectional SEM images of 8 minutes annealed sample.

It is clear that the alignment of CNTs are similar independent of the annealing time. The nanoparticle formation is uniform and well distributed among the surface of the foils. It is supposed that the nanoparticles are formed on the substrate rather than gathering to form bigger nanoparticles or diffusing towards the substrate with time. Raman spectra of these samples are provided in Figure 5.22.

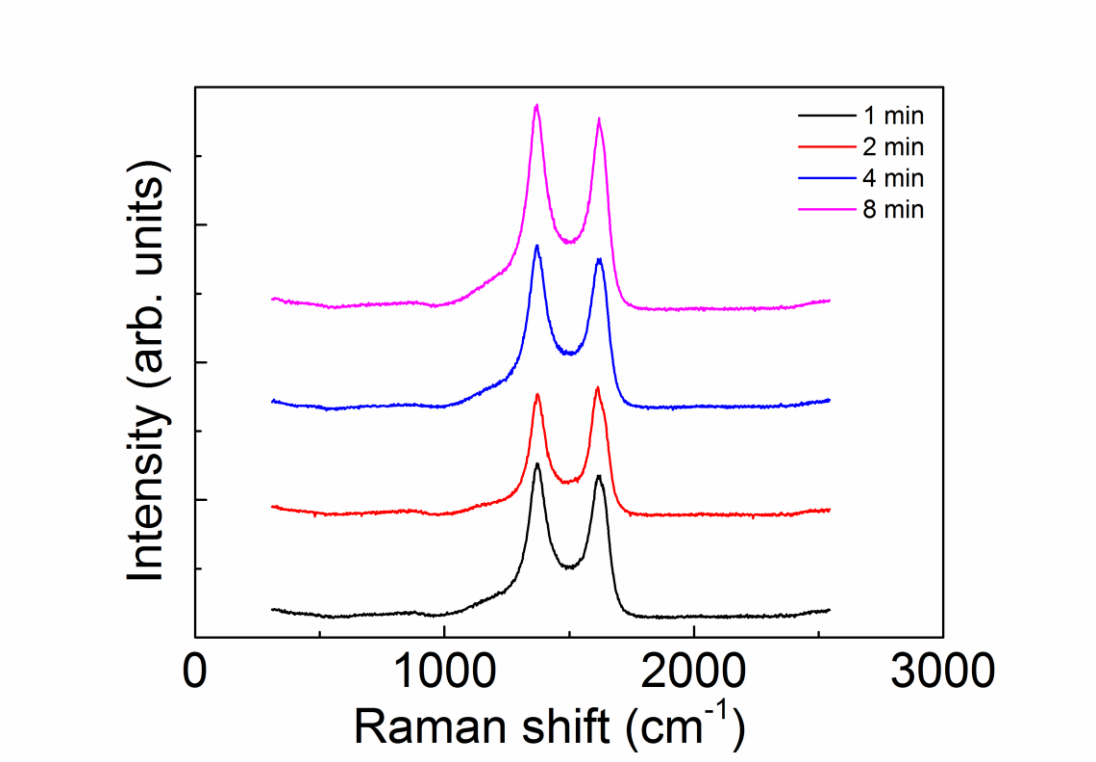

Figure 5.22 Raman spectra of the CNTs grown using different annealing times.

Not much of a difference was observed from the Raman spectra of the samples, in consistence with the SEM images.

5.2 Electrochemical Measurements

In this part of the thesis, electrochemical characteristics of some of the samples mentioned in Section 5.1 are discussed. As an electrolytic solution, 1 M sodium sulfate (Na_2SO_4) is prepared. For the measurements, Ag/AgCl reference electrode, platinum foil counter electrode and CNT/aluminum foil sample as the working electrode are immersed within the electrolyte in a three-electrode configuration.

5.2.1 Effect of Catalyst and Substrate on the Electrochemical Characteristics

Substrates with CNTs grown using USP and PVD deposited catalyst on both pure and kitchen aluminum foils were subjected to electrochemical measurements. In order to understand the effect of catalyst and substrate type on electrochemical characteristics, substrates with the same sizes that were subjected to CNT growth with the same recipes were used. The SEM images and Raman spectra of these four samples are provided in Figures 5.4 and 5.5, respectively. The cyclic voltammetry (CV) measurements were conducted at a scan rate of 800 mV/s. The potential interval is determined as 0 - 0.8 V. Results of the measurements are provided in Figure 5.23.

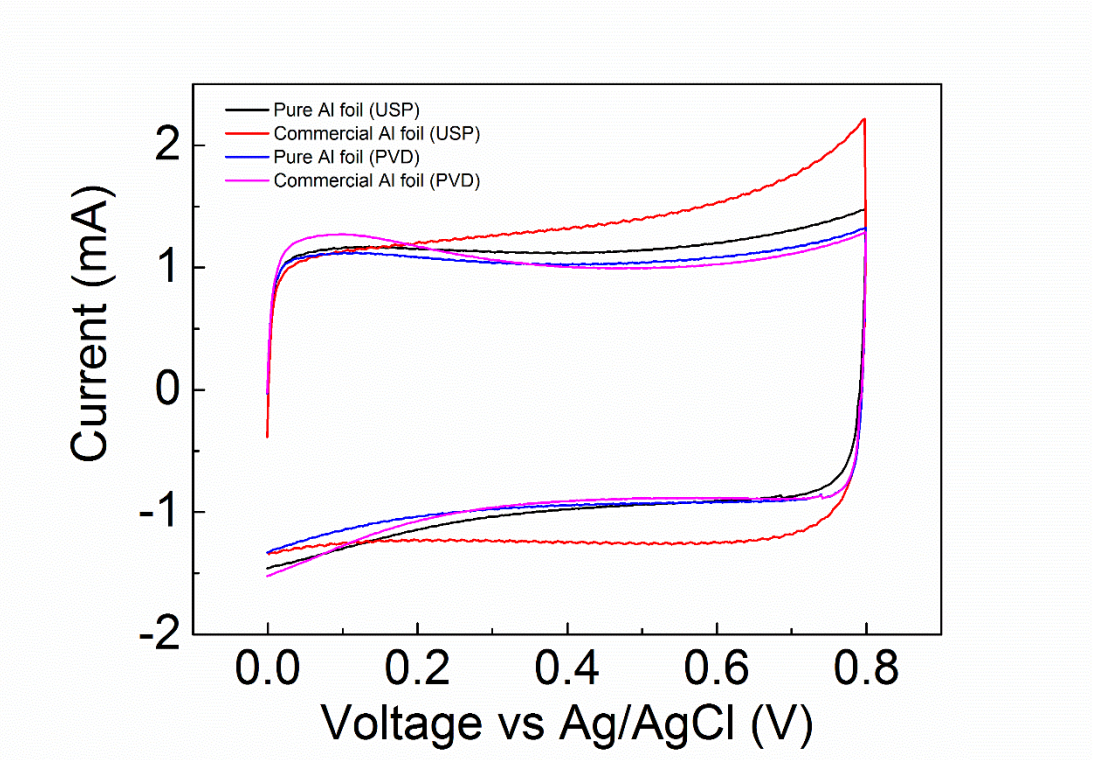

Figure 5.23 CV characteristics showing the effect of different catalyst and substrate types at a scan rate of 800 mV/s.

The corresponding capacitance values of the samples are shown in Table 5.2.

Table 5.2 Capacitance values of the samples with different catalysts and substrates.

Sample	Capacitance (mF/cm^2)
Pure aluminum foil, catalyst deposited via USP	2.19
Kitchen aluminum foil, catalyst deposited via USP	3.19
Pure aluminum foil, catalyst deposited via PVD	2.06
Kitchen aluminum foil, catalyst deposited via PVD	2.09

In the literature, the specific capacitance values of VACNTs on aluminum substrates are range between 25-80 F/g [48] [71]. When the results of these samples are compared in terms of mF/cm^2 unit, which are 7-13 mF/cm^2, it can be concluded CNT lengths are directly related with specific capacitances since these values are belong to CNTs up to 80 μm.

The CV measurements of these four electrode samples show similar capacitive properties. These samples are reproduced multiple of times so does the CV measurements. Although there were slight changes, similar results were obtained. These minor changes can be attributed to the flexible nature of the aluminum foils. It is almost impossible to adjust the immersed CNT surface area and the exact distance between counter and the working electrode during each measurement.

These four samples are also subjected to galvanostatic charge discharge (GCD) measurements and the results are provided in Figure 5.24. Measurements are made at five different current densities of 100, 250, 500 $\mu A/cm^2$, 1 and 2 mA/cm^2.

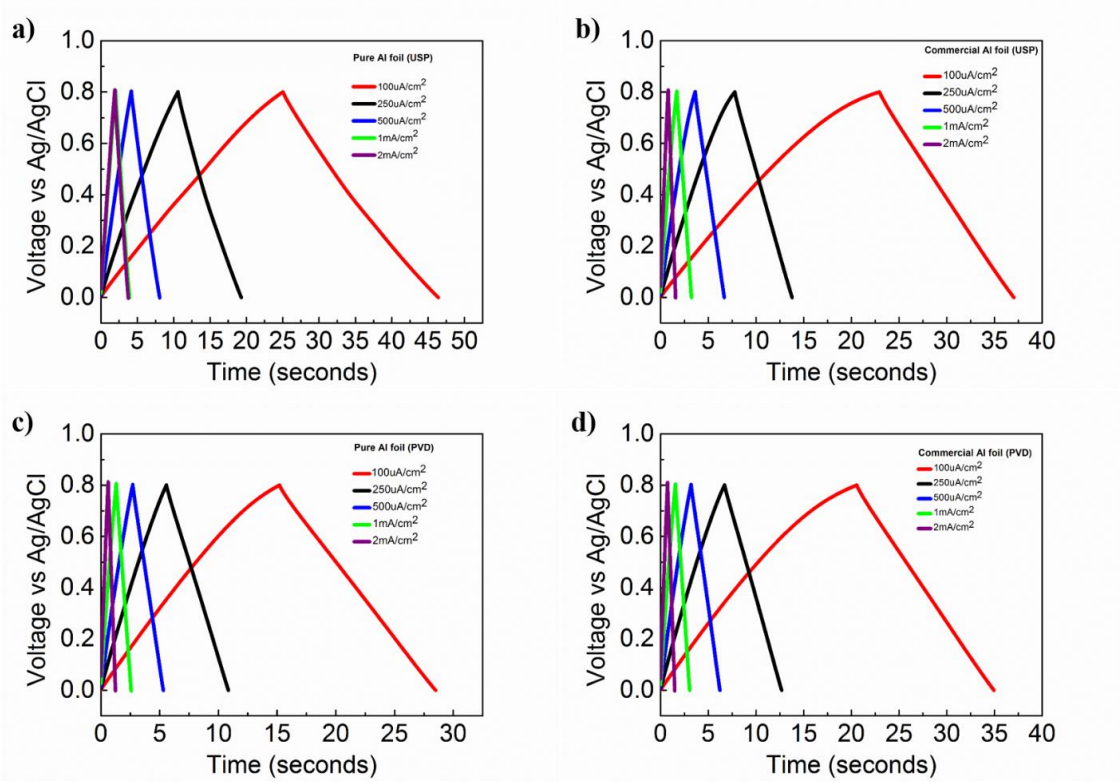

Figure 5.24 Galvanostatic chage-discharge characteristics of CNTs on (a) pure aluminum foil, catalyst deposited via USP, (b) commercial aluminum foil, catalyst deposited via USP, (c) pure aluminum foil, catalyst deposited via PVD and (d) commercial aluminum foil, catalyst deposited via PVD.

The change in voltage with time for both charging and discharging shows a symmetric and linear profile, which was typical of electric double layer supercapacitors. In addition, there was no major voltage drop, showing that there was nearly no internal resistance. This is particularly important for the electrodes fabricated using CNTs. For CNT based electrodes, if CNTs are deposited onto a conducting substrate, series resistance always occurs resulting from the interface between the substrate and the CNTs. However, in this case, since VACNTs that were directly grown on aluminum

foils, series resistance was almost negligible. This makes direct, one-step growth of VACNTs on metal foils an important route to fabricate supercapacitor electrodes.

Impedance measurements on these four samples were also conducted. The corresponding Nyquist plots within a frequency range of 50 kHz - 50 mHz is provided in Figure 5.25

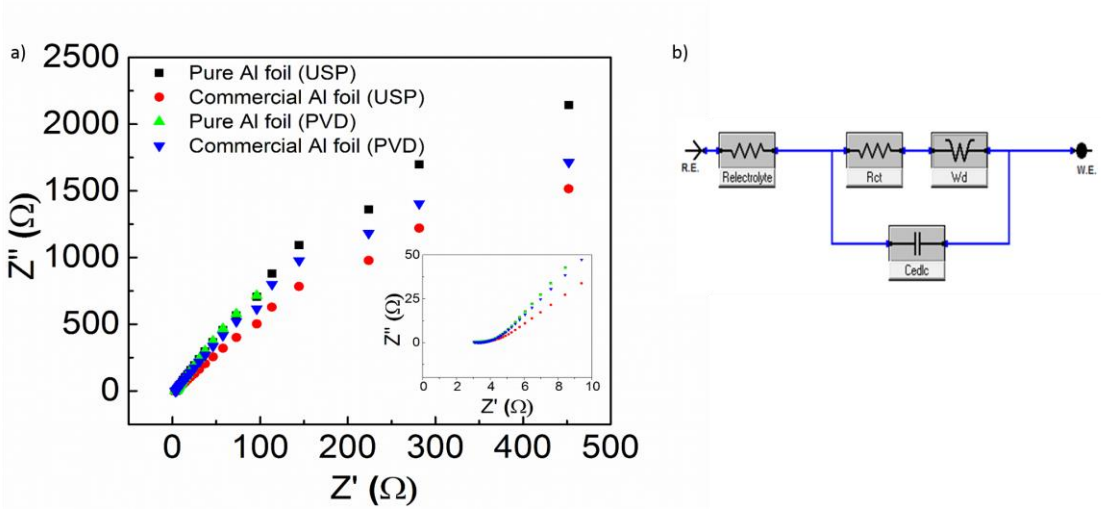

Figure 5.25 (a) Impedance spectra of the electrodes measured within the range of 50 kHz to 50 mHz. (b) Impedance model used for the analysis.

Consistent with the Figure 5.24, the highest slope, indicating the largest capacitance, was obtained for pure aluminum foil with catalyst deposited via USP method. Supercapacitors behave as a resistance and capacitance in the high and low frequency region, respectively. The nearly vertical lines, parallel to imaginary axis, in Nyquist plot represent the ideal supercapacitor behavior and the absence of semicircles in high frequency region indicate that there are no charge transfer resistances. The intersecting points with real axis in the high frequency region points the internal resistance of the

electrodes, which are less than 3 Ω in this case. Absence of the semicircles show that the charge transfer resistance between the electrode and electrolyte is almost negligible. As discussed before, one-step and direct growth of VACNTs on aluminum foils initiates good contacts between the CNTs and underlying aluminum foils and the electrodes formed with this method possess ideal supercapacitor characteristics. A typical equivalent circuit of the fabricated electrodes can be seen in Figure 5.25 (b). Although it gives an impression on how the charge storage affected by components such as the internal resistance or diffusion of ions, a real case is much more complicated. Complexity arises from the fact that the VACNTs create numerous parallel capacitive components on the aluminum foils.

For further analysis, change in specific capacitance and coulombic efficiency within the supercapacitor electrodes during 300 charge/discharge cycles were measured. Cyclic performance of the electrodes is provided in Figure 5.26. Electrode samples were charged and discharged at a current density of 2 mA/cm^2.

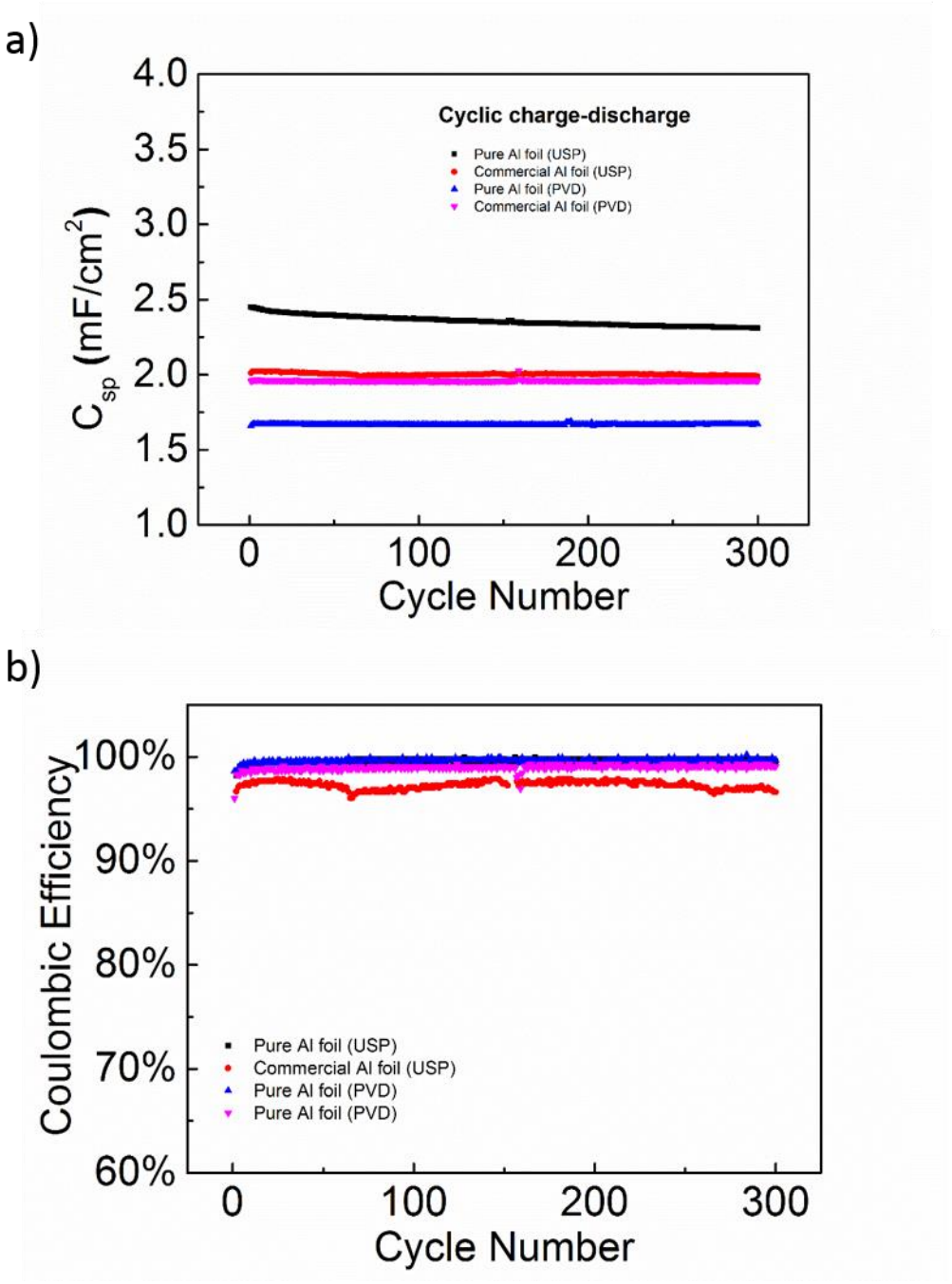

Figure 5.26 Cycling performance with respect to (a) specific capacitance and (b) coulombic efficiency of the samples measured through constant current charge - discharge at a current density of 2 mA/cm^2.

There was almost no variation in capacitance for 300 cycles. This is clearly showing the electrochemical as well as mechanical stability of the VACNTs on aluminum foils. Moreover, coulombic efficiencies were almost 100% for all the investigated samples. Although further cycling measurements (for at least 10000 cycles) are necessary to truly confirm this, reported values are indicating the potential of the fabricated VACNTs on aluminum foils as supercapacitor electrodes.

5.2.2 Effect of CNT Growth Temperature on the Electrochemical Characteristics

In this part, aluminum foils with CNTs grown at different temperatures were tested for their electrochemical performance. CNTs grown on pure aluminum foil using the catalyst deposited via USP method were used for the measurements. CNTs grown at temperatures of 600, 610, 620 and 630°C were utilized. SEM images and Raman spectra of these samples have already been provided in Figures 5.7 and 5.9, respectively. The length of the CNTs were increased with temperature till 620°C. As the CNTs were exposed to higher temperatures, they got entangled and the substrate got spoiled. That is the reason why CNTs grown at 630°C appeared shorter than their actual length as they were bent and curved. Figure 5.27 shows the cyclic voltammetry results of the samples.

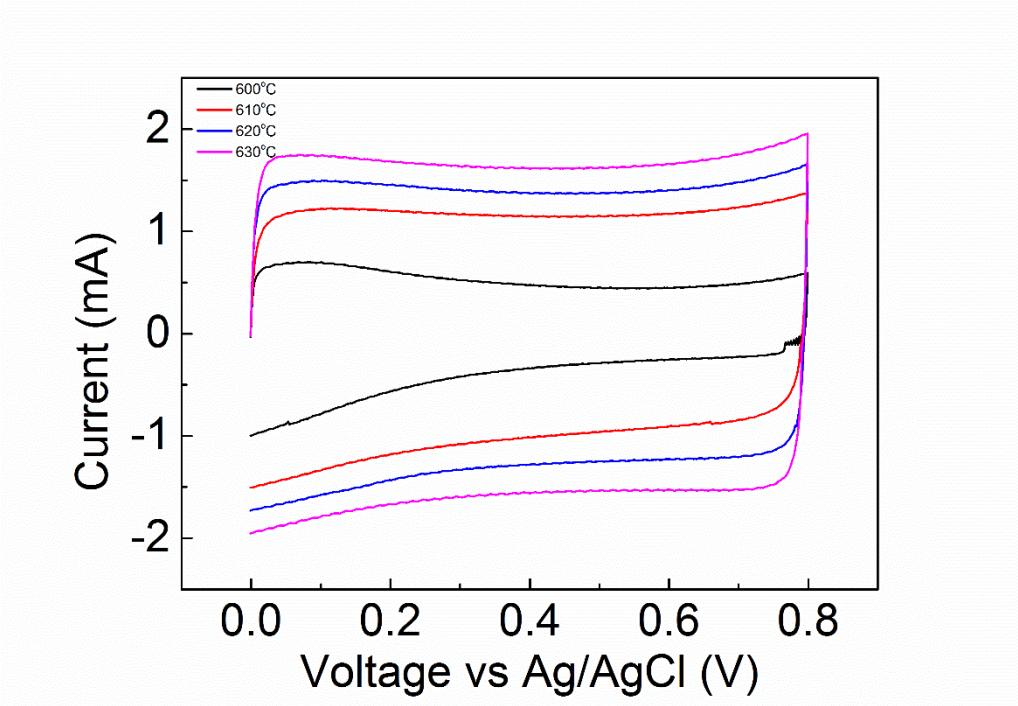

Figure 5.27 Cyclic voltammetry results of the electrodes prepared at different temperatures at a scan rate of 800 mV/s.

When the SEM images and CV characteristics of these samples are compared, it is apparent that the capacity of the electrodes increases with the length of the CNTs. This is because the total surface area of the electrodes increases with the CNT length.

5.2.3 Effect of Flexing on the Electrochemical Characteristics

Growth of VACNTs on aluminum foils adds function to the foils, while still conserving their mechanical flexibility. Thus, it is possible to fabricate flexible supercapacitors using the VACNTs on aluminum foils. Aluminum foil is one of the best flexible current collectors known that is cheap and readily available. For flexed electrochemical measurements, CNTs grown on pure aluminum foils with USP

deposited catalyst were used. During CNT growth, hydrogen flow rate, pressure and growth temperature of the sample was 200 sccm, 8 mbars and 620°C, respectively. Electrochemical measurements were performed within a potential window of 0 and 0.8 V. Figure 5.28 shows the cyclic voltammetry results of the electrode at different scan rates from 50 mV/s up to 800 mV/s.

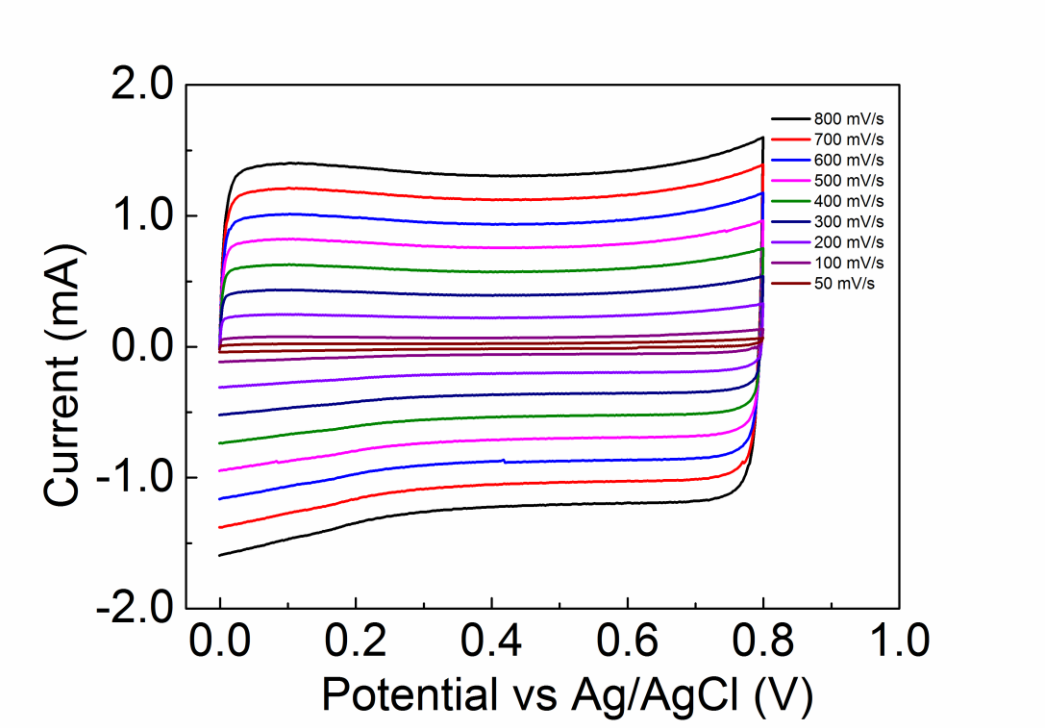

Figure 5.28 Cyclic voltammetry results of the VACNT electrodes at different scan rates.

Areal capacitance values of the VACNT electrode at scan rates of 50, 100, 200, 300, 400, 500, 600, 700 and 800 mV/s are 0.35, 0.73, 0.39, 0.71, 1.15, 1.8, 2.15, 2.33, 2.45, 2.52, 2.57 and 2.61 mF/cm^2 respectively.

To determine the mechanical performance of the electrodes, a custom build mechanical system was used. The sample (*2 cm x 1 cm* in size) was attached to the system from its short edges, as seen in Figure 5.28 (a). The bending diameter was determined as 7.5 mm, set by the sample holding heads. Moreover, VACNTs on flat and bent aluminum foils are schematically demonstrated in Figure 5.28 (c).

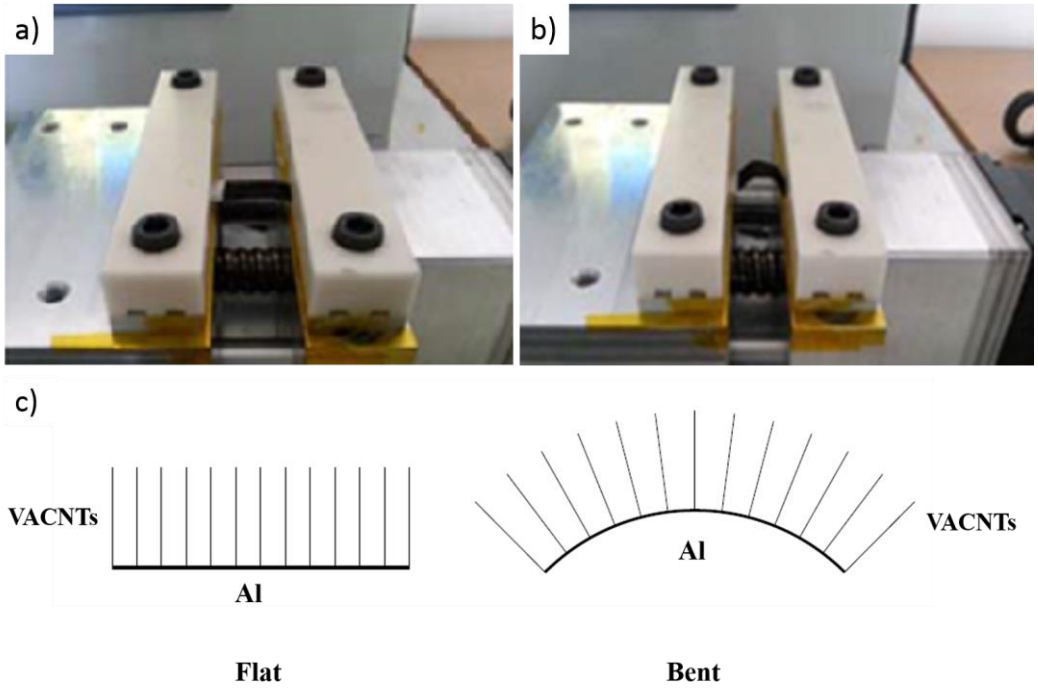

Figure 5.29 Photographs of the bending setup for (a) straight and (b) bent sample with VACNTs. (c) Schematics of VACNTs on flat and bent aluminum foils.

First, the CV measurement of the as-grown sample (denoted as 0 bending) was carried out. Then the foil was bent for 500 times and electrochemically tested again. This bending and measuring processes were repeated for 1000, 1500 and 2000 times. The

CV graph of the sample at the end of each 500 bending cycles can be seen in Figure 5.30.

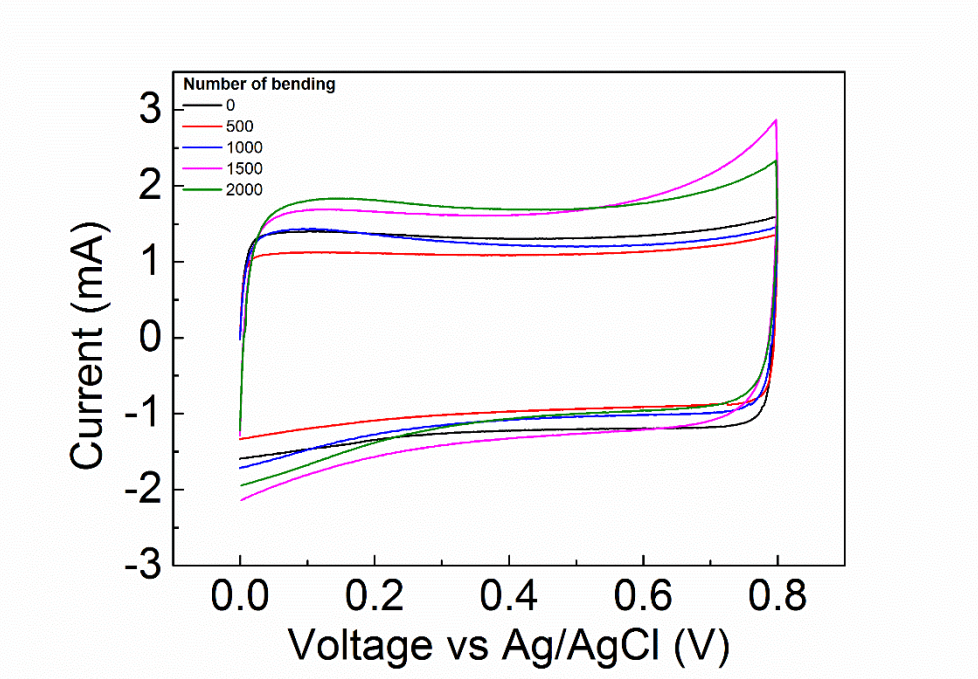

Figure 5.30 CV results of the electrodes after each 500 bending cycles at a scan rate of 800 mV/s.

Similar CV characteristics were obtained for the samples, independent of the number of bending cycles. Bending operation with the set radius of curvature deformed the foil after 2000 cycles, thus the maximum number of bending cycles was designed as 2000 times. Therefore, it is the aluminum foil not the CNTs that limit the flexibility of the electrodes. All in all, obtained results are quite promising, showing the potential of fabricated samples as flexible supercapacitor electrodes.

In the literature, the bending cycle of the flexible supercapacitor electrodes that are carbon or nanocomposite based is up to 1000 where the electrodes are at least slightly affected [72] [73] [74].

CHAPTER 6

CONCLUSIONS AND FUTURE WORK

In this work, first, the CNT growth on aluminum foil using CVD method is investigated in detail. Aluminum is preferred as a cheap, flexible, conductive and readily available substrate for the CNT growth. The effect of each growth parameter was investigated, while the other parameters were kept unchanged. In brief, the catalyst and substrate type, catalyst thickness in addition to the effect of CVD parameters such as temperature, pressure, gas flow rates and annealing parameters were evaluated. It was summarized that each parameter in one way or another depend on the others and changing one parameter affects them all. Each substrate and each catalyst type and catalyst thickness had its own recipe. During experiments, numerous numbers of USP and PVD deposited catalysts on aluminum foils were used and compared. It was observed that the USP deposited catalysts could give similar results with PVD deposited counterparts, which is an alternatively easy, vacuum-free and cost-effective method. In addition, deposition over large areas is also possible with the USP method.

In the second part of the thesis, supercapacitors were fabricated using the electrodes fabricated in the first part. The effect of catalyst type, catalyst deposition method and the CNT length on the electrochemical characteristics of the electrodes were

investigated. The increase in the electrode surface area correlated with an increase in the CNT length resulted in an increase in the capacitance of the electrodes.

Finally, the CNTs grown on aluminum foil with catalyst deposited via USP were tested in terms of their flexibility. Although they were bent for 2000 times, they preserved their electrochemical performance.

In this thesis, it was observed that the CNTs could be grown on a desired area of the substrate, where the growth process is adaptable to a number of different substrates. It might be interesting to investigate other conductive substrates than aluminum foils using similar growth steps.

In this work, only one-electrode measurements were made. It will be intriguing to fabricate full devices with 2 symmetric electrodes and measure their characteristics both when straight and bent.

Last but not least, electrolytes different than sodium sulfate can be used to investigate the performance of the VACNT electrodes. Acidic and basic electrolytes cannot be used due to the current collecting metallic foils. However, the effect of aqueous cationic electrolytes (i.e. lithium sulfate (Li_2SO_4), potassium sulfate (K_2SO_4)) and anionic electrolytes (i.e. potassium chloride (KCl) and potassium iodide (KI)) can be investigated.

REFERENCES

[1] A. Mamalis, L. Vogtländer and A. Markopoulos, "Nanotechnology and nanostructured materials: trends in carbon nanotubes," *Elsevier,* pp. 16-30, 2002.

[2] E. H. Falcao and F. Wudl, "Carbon allotropes: beyond graphite and diamond," *Journal of Chemical Technology and Biotechnology*, vol. 82, no. 6, p. 524–531, 2007.

[3] Q. Zhang, "Carbon Nanotubes and Their Applications," Pan Stanford Publishing Pte. Ltd., 2012, p. 2.

[4] H. O. Pierson, Handbook of Carbon, Graphite, Diamond and Fullerenes: Properties, Processing and Applications, New Jersey: Noyes Publications, 1993.

[5] M. Scarselli, P. Castrucci and M. D. Crezcenzi, "Electronic and optoelectronic nano-devices based on carbon nanotubes," *IOPscience,* 2012.

[6] A. K. Geim, "Graphene: Status and Prospects," vol. 324, no. 5934, 2009.

[7] A. H. C. Neto, F. Guinea, N. M. R. Peres, A. S. Novoselov and A. K. Geim, "The electronic properties of graphene," no. 81, 2009.

[8] Z. Liu, Y. Wang, Z. Xiaoliang, Y. Xu, Y. Chen and J. Tian, "Nonlinear optical properties of graphene oxide in nanosecond and picosecond regimes," no. 94, 2009.

[9] S. Iijima, "Helical microtubules of graphitic carbon," vol. 354, 1991.

[10] M. Kumar and Y. Ando, "Chemical Vapor Deposition of Carbon Nanotubes:A Review on Growth Mechanism and Mass Production," 2010.

[11] R. K. A. Al-Rub, A. I. Ashour and B. M. Tyson, "On the aspect ratio effect of multi-walled carbon nanotube reinforcementson the mechanical properties of cementitious nanocomposites," *Elsevier*, pp. 647-655, 2012.

[12] M. A. Pulickel and Z. Z. Otto, "Applications of carbon nanotubes," 2001.

[13] P. R. Bandaru, "Electrical Properties and Applications of Carbon Nanotube Structures," *Journal of Nanoscience and Nanotechnology*, pp. 1-29, 2007.

[14] M. P. Anantram and F. Leonard, "Physics of carbon nanotube electronic devices," *IOPScience*, 2006.

[15] K.-T. Lau and D. Hui, "The revolutionary creation of new advanced materials-carbon nanotube composites," *Elsevier*, 2002.

[16] N. B. Singh and S. Agrawal, "Foldvarı Group," [Online]. Available: https://uwaterloo.ca/foldvari-group/research-program/drug-delivery. [Accessed 30 May 2015].

[17] H. Omachi, T. Nakayama, E. Takahashi, Y. Segawa and K. Itami, "Initiation of carbon nanotube growth by well-defined carbon nanorings," *Nature Chemistry*, 2013.

[18] Y. Ando and X. Zhao, "Synthesis of Carbon Nanotubes by Arc-Discharge Method," *New Diamond and Frontier Carbon Technology*, 2006.

[19] M. M. A. Rafique and J. Iqbal, "Production of Carbon Nanotube by Different Routes-A Review," *Journal of Encapsulation and Adsorption Sciences*, pp. 29-34, 2011.

[20] C. D. Scott, S. Arepalli, P. Nikolaev and R. E. Smalley, "Growth mechanism for single-wall carbon nanotubes is a laser-ablation process," *Applied Physics A* , pp. 573-580, 2001.

[21] N. Yoshikawa, T. Asari, N. Kishi, S. Hayashi, S. Toshiki and H. Shinohara, "An efficient fabrication of vertically aligned carbon nanotubes on flexible aluminium foils by catalyst-supported chemical vapor deposition," 2008.

[22] Y. Yu, C. Cui, W. Qian, Q. Xie, C. Zheng, C. Kong and F. Wei, "Carbon nanotube production and application in energy storage," 2012.

[23] M. Meyyapan, L. Delzeit, A. Cassell and D. Hash, "Carbon nanotube growth by PECVD: a review," 2002.

[24] S. Esconjauregiu, S. Bhardway, J. Yang, C. Castellarin-Cudia, R. Xie, L. D'Arsie, T. Makaryan, H. Sugime, S. Eslava, C. Cepek and J. Robertson, "Carbon nanotube growth on conductors: Influence of the support structure and catalyst thickness," 2014.

[25] C. J. Lee, D. W. Kim, T. J. Lee, Y. C. Choi, Y. S. Park, Y. H. Lee, W. B. Choi, N. S. Lee, G.-S. Park and J. M. Kim, "Synthesis of aligned carbon nanotubes using thermal chemical vapor deposition," vol. 1999, 1999.

[26] M. Hiramatsu and M. Hori, "Aligned Growth of Single-Walled and Double-Walled Carbon Nanotube Films by Control of Catalyst Preparation," 2011.

[27] K. P. S. S. Hembram, K. R. Reddy and G. M. Rao, "Geometrical Modeling of Walls of Multiwall Carbon Nanotube," 2013.

[28] C. Mattevi, C. T. Wirth, S. Hofmann, R. Blume, M. Cantoro, C. Ducati, C. Cepek, A. Knop-Gericke, S. Milne, C. Castellarin-Cudia, S. Dolafi, A. Goldoni, R. Schloegl and J. Robertson, "X-ray Photoelectron Spectroscopy Study of Catalyst-Support Interactions and Growth of Carbon Nanotube Forests," 2008.

[29] C. J. Lee, J. Park and J. A. Yu, "Catalyst effect on carbon nanotubes synthesized by thermal chemical vapor deposition," *Elsevier,* 2002.

[30] G. Zhong, J. H. Warner, M. Fouquet, A. W. Robertson, B. Chen and J. Robertson, "Growth of Ultrahigh Density Single-Walled Carbon Nanotube Forests by Improved Catalyst Design," 2012.

[31] H. Chen, A. Roy, J.-B. Baek, L. Zhu, J. Qu and L. Dai, "Controlled growth and modification of vertically-aligned carbon nanotubes for multifunctional applications," *Elsevier,* pp. 63-91, 2010.

[32] "Solpower Processing," [Online]. Available: https://stuff.mit.edu/afs/athena.mit.edu/course/3/3.082/www/team2_f02/Pages/processing.html. [Accessed 20 December 2015].

[33] Lado Filipovic, [Online]. Available: http://www.iue.tuwien.ac.at/phd/filipovic/node56.html. [Accessed 20 December 2015].

[34] C. T. Wirth, C. Zhang, G. Zhong, S. Hofmann and J. Robertson, "Diffusion and Reaction Limited Growth of Carbon Nanotube Forests," 2009.

[35] T. D. Makris, L. Giorgi, N. Giorgi, N. Lisi and E. Salernitano, "CNT growth on alumina supported nickel catalyst by thermal CVD," vol. 14, no. 3-7, 2005.

[36] J. D. Plummer, M. D. Deal and P. B. Griffin, Silicon VLSI Technology: Fundamentals, Practice and Modeling, Upper Saddle River NJ: Prentice Hall, 2000.

[37] C. H. Li, S. C. Tseng, S. C. Lo, K. F. Chen, Z. Y. Juang, K. C. Leou and C. H. Tsai, "Pressure effect of low-temperature growth of multi-wall carbon nanotubes on Nickel catalyst/barrier-coated glass by thermal-CVD," 2006.

[38] W. Z. Li, J. G. Wen, Y. Tu and Z. F. Ren, "Effect of gas pressure on the growth and structure of carbon nanotubes by chemical vapor deposition," 2001.

[39] C. J. Lee, J. Park, Y. Huh and J. Y. Lee, "Temperature effect on the growth of carbon nanotubes using thermal chemical vapor deposition," *Elsevier,* 2001.

[40] H. Cui, G. Eres, J. Y. Howe, A. Puretkzy, M. Varela, D. B. Geohegan and D. H. Lowndes, "Growth behavior of carbon nanotubes on multilayered metal catalyst film in chemical vapor deposition," 2002.

[41] Q. Weizhong, T. Liu, F. Wei, Z. Wang and Y. Li, "Enhanced production of carbon nanotubes: combination of catalyst reduction and methane decomposition," 2003.

[42] M. J. Bronikowski, "CVD growth of carbon nanotube bundle arrays," 2006.

[43] C. Lu and J. Liu, "Controlling the Diameter of Carbon Nanotubes in Chemical Vapor Deposition Method by Carbon Feeding," *J. Phys. Chem. B,* pp. 20254-20257, 2006.

[44] A. K. Chakraborty, J. Jacobs, C. Anderson, C. J. Roberts and M. R. C. Hunt, "Chemical vapor deposition growth of carbon nanotubes on Si substrates using Fe catalyst: What happens at the nanotube/Fe/Si interface," 2006.

[45] F. Ohashi, G. Y. Chen, V. Stolojan and S. R. P. Silva, "The role of the gas species on the formation of carbon nanotubes during thermal chemical vapour deposition," 2008.

[46] M. J. Behr, E. A. Gaulding, K. A. Mkhoyan and E. S. Aydil, "Effect of hydrogen on catalyst nanoparticles in carbon nanotube growth," 2010.

[47] G. D. Nessim, "Properties, synthesis, and growth mechanisms of carbon nanotubes with special focus on thermal chemical vapor deposition," 2010.

[48] S. Dörfler, I. Felhösi, T. Marek, S. Thieme, H. Althues, L. Nyikos and S. Kaskel, "High power supercap electrodes based on vertical aligned carbon nanotubes on aluminum," 2013.

[49] F. Zhao, A. Vicenzo, M. Hashempour and M. Bestetti, "Supercapacitor electrodes by direct growth of multi-walled carbon nanotubes on Al: a study of performance versus layer growth evolution," 2014.

[50] R. H. Baughman, A. A. Zakhidov and W. A. de Heer, "Carbon Nanotubes-the Route Toward Applications," 2002.

[51] N. S. Lee, D. S. Chung, I. T. Han, J. H. Kang, Y. S. Choi, H. Y. Kim, S. H. Park, W. K. Jin, M. J. Yun, J. E. Jung, C. J. Lee, J. H. You, S. H. Jo, C. G. Lee and J. M. Kim, "Application of carbon nanotubes to field emission displays," 2001.

[52] A. P. Graham, G. S. Duesberg, R. V. Seidel, M. Liebau, E. Unger, W. Pamler, F. Kreupl and W. Hoenlein, "Carbon Nanotubes for Microelectronics".

[53] P. L. McEuen, "Carbon-based electronics," vol. 393, 1998.

[54] H. He, L. A. Pham-Huy, P. Dramou, D. Xiao and C. Pham-Huy, "Carbon Nanotubes: Applications in Pharmacy and Medicine," 2013.

[55] "Capacitance and Dielectrics," [Online]. Available: http://web.mit.edu/viz/EM/visualizations/coursenotes/modules/guide05.pdf. [Accessed 20 June 2015].

[56] A. G. Pandolfo and A. F. Hollenkamp, "Carbon properties and their role in supercapacitors," 2006.

[57] A. Schneuwly and R. Gallay, "Properties and applications of supercapacitors From the state-of-the-art to future trends," 2000.

[58] L. L. Zhang and X. S. Zhao, "Carbon-based materials as supercapacitor electrodes," 2009.

[59] S. Bose, T. Kuila, A. K. Mishra, R. Rajasekar, N. H. Kim and J. H. Lee, "Carbon-based nanostructured materials and their composites as supercapacitor electrodes," vol. 22.

[60] A. B. Fuertes, F. Pico and J. M. Rojo, "Influence of pore structure on electric double-layer capacitance of template mesoporous carbons," 2004.

[61] N. Kularatna, Energy Storage Deviced for Electronic Systems: Rechargeable Batteries and Supercapacitors, Academic Press, 2015.

[62] N.-S. Choi, Z. Chen, S. A. Freunberger, X. Ji, Y.-K. Sun, K. Amine, G. Yushin, L. F. Nazar, J. Cho and P. G. Bruce, "Challenges Facing Lithium Batteries and Electrical Double-Layer Capacitors," 2012.

[63] O. Barbieri, M. Hahn, A. Herzog and R. Kötz, "Capacitance limits of high surface area activated carbons for double layer capacitors," 2005.

[64] W. Lu and R. Hartman, "Nanocomposite Electrodes for High-Performance Supercapacitors," 2011.

[65] "UW Laboratory for Emerging Energy Research," [Online]. Available: http://www.leer.uwaterloo.ca/research.html. [Accessed 5 August 2015].

[66] E. Frackowiak and F. Be´guin, "Carbon materials for the electrochemical storage of energy in," vol. Carbon 39, 2001.

[67] F. Béguin, E. Raymundo-Piñero and E. Frackowiak, "Electrical Double-Layer Capacitors and Pseudocapacitors," in *Carbons for electrochemical energy storage and conversion systems*, CRC Press, 2010.

[68] M. S. Halper and J. C. Ellenbogen, "Supercapacitors: A Brief Overview," MITRE Nanosystems group, Virginia, 2006.

[69] S. Gouws, "Voltammetric Characterization Methods for the PEM Evaluation of Catalysts," in *Electrolysis*, 2012.

[70] "Gamry Instruments application notes," GAMRY INSTRUMENTS, [Online]. Available: http://www.gamry.com/application-notes/electrodes-cells/two-three-and-four-electrode-experiments/. [Accessed 10 October 2015].

[71] R. Reit, J. Nguyen and W. J. Ready, "Growth time performance dependence of vertically aligned carbon nanotube supercapacitors grown on aluminum substrates," *Elsevier*, vol. 91, pp. 96-100, 2013.

[72] M. F. El-Kady, V. Strong, S. Dubin and R. B. Kaner, "Laser Scribing of High-Performance and Flexible Graphene-Based Electrochemical Capacitors," *Science*, vol. 335, no. 6074, pp. 1326-1330, 2012.

[73] Y. He, W. Chen, X. Li, Z. Zhang, J. Fu, C. Zhao and E. Xie, "Freestanding Three-Dimensional Graphene/MnO2 Composite Networks As Ultralight and Flexible Supercapacitor Electrodes," *ACS nano*, vol. 7, no. 1, pp. 174-182, 2012.

[74] Y. Xu, Z. Lin, X. Huang, Y. Liu, Y. Huang and X. Duan, "Flexible Solid-State Supercapacitors Based on Three-Dimensional Graphene Hydrogel Films," *Acs Nano*, vol. 7, no. 5, pp. 4042-4049, 2013.